University of Nevada, Reno

Investigation of the Influence of Temperature Inversions and Turbulence on Land-atmosphere Interactions for Rolling Terrain

A thesis submitted in partial fulfillment of the requirements for the degree of Master of Science in Atmospheric Science

By

Olabosipo O. Osibanjo

Dr. Heather A. Holmes/Thesis Advisor

August, 2016

THE GRADUATE SCHOOL

We recommend that the thesis
prepared under our supervision by

OLABOSIPO O. OSIBANJO

Entitled

Investigation Of The Influence Of Temperature Inversions And Turbulence On Land-Atmosphere Interactions For Rolling Terrain

be accepted in partial fulfillment of the
requirements for the degree of

MASTER OF SCIENCE

Heather A. Holmes, Phd., Advisor

Patrick W. Arnott, Phd., Committee Member

Jaime Barnard, Phd., Graduate School Representative

David W. Zeh, Ph.D., Dean, Graduate School

August, 2016

Abstract

The surface-atmosphere exchange of trace gases and energy is important as it impacts weather, climate, and air quality. The models used for estimating surface fluxes such as heat, moisture, and carbon dioxide (CO_2) were designed to work best in horizontally uniform, flat terrain. This is a challenge for measuring surface fluxes in non-uniform, complex terrain as these models break down especially during stable atmospheric conditions. The complex terrain generates its own thermal circulation such as the drainage flow at nighttime. Surface heterogeneity is common in complex terrain, which is one of the factors that leads to erroneous surface fluxes estimation. The concentrations of atmospheric greenhouse gases are increasing, leading to changes in atmospheric boundary layer (ABL) dynamics as a result of the changing surface energy balance. The ABL processes are important to characterize because they are difficult to parameterize in global and regional scale atmospheric models. Empirical data can be collected using eddy covariance micrometeorological methods to measure turbulent fluxes (e.g., sensible heat, moisture, and CO_2) and quantify the land-atmosphere exchange.

The objectives of this work are to calculate surface fluxes for rolling terrain using observational data collected during one week in September 2014 from a monitoring site in Echo, Oregon and to investigate the log law in the ABL. The site is located in the Columbia Basin with rolling terrain, irrigated farmland, and over 100 wind turbines. The 10 m tower was placed in a small valley depression to isolate nighttime temperature inversions. This thesis presents observations of momentum, sensible heat, moisture, and

CO_2 fluxes from data collected at a sampling frequency of 10Hz at four heights. Results show a strong correlation between temperature inversions and CO_2 flux. The log layer could not be achieved as the value of the estimated von Karman constant (~0.62) is not close to that of the accepted value of 0.41. The impact of the irrigated farmland near the measurement site was observed in the latent heat flux, where the advection of moisture was evident in the tower moisture gradient. A strong relationship was also observed between fluxes of sensible heat, latent heat, CO_2, and atmospheric stability. The average nighttime CO_2 concentration observed was ~407 ppm, and daytime ~388 ppm compared to the 2013 global average CO_2 concentration of 395 ppm. The maximum CO_2 concentration (~485 ppm) was observed on the strongest temperature inversion night. There are few uncertainties in the measurements. The manufacturer for the eddy covariance instruments (EC 150) quotes uncertainty of $\pm\ 0.1°C$ for temperature between -0$°C$-40$°C$. Error bars were generated on the estimated surface sensible heat flux using the standard deviation and mean values. Under the most stable atmospheric conditions, uncertainty (assumed to be the variability in the flux estimates) was close to the minimum (~$\pm\ 5\ W\ m^{-2}$).

Acknowledgements and Dedication

I would like to thank the almighty God for seeing me through this journey. I would like to acknowledge Dr. Chad Higgins and his research group at Oregon State University for collaborating on the field experiment that collected the data for this research. I would like to thank my advisor, Dr. Heather Holmes for giving me this research opportunity and her endless support towards the success of this project. I would also like to appreciate my advisory committee members, Dr. W. Patrick Arnott, and Dr. Jaime Barnard for providing many insightful suggestions to my study.

I would like to thank Dr. Mark Green for giving me grants through the Division of Atmospheric Sciences (DAS) at Desert Research Institute, making the completion of my program fast without any financial struggle.

Many people contributed throughout the project, especially Dr. Segun Ogunjemiyo from California State University, Fresno, S. Marcela Loria-Salazar from Atmospheric Sciences department at University of Nevada Reno. I appreciate your help.

Lastly, I thank my family for all the love and support. Your moral support and encouragement keeps me going.

Table of Contents

List of Figures

Chapter 1: Introduction

1.1 Background

The surface-atmosphere exchange of trace gases and energy is important as it impacts climate and human health. The models used for estimating surface fluxes such as heat, moisture, and carbon dioxide (CO_2) were designed to work best on horizontally uniform, flat terrain [Businger et al., 1971; Brutsaert, 1998]. However, measuring surface fluxes on non-uniform, complex terrain presents a challenge as the models designed for flat terrain break down, especially during stable atmospheric conditions because surface fluxes are usually underestimated during stable atmospheric conditions. The exchange of CO_2 and water vapour (H_2O) between the earth surface and atmosphere influences the weather and climate, hence monitoring these trace species is crucial. Human activities have been a major contributor to the steady increase in the concentration of CO_2 in the atmosphere, which impacts the climate. H_2O and CO_2 are the most important greenhouse gases that absorb radiation emitted by Earth's surface and re-radiate heat back to the ground thereby, causing the Earth's surface temperature to be warmer than normal—a phenomenon known as Greenhouse Effect [Whiteman 2000].

Scientists are expected to play a major role in evaluating the impact of anthropogenic activities on the environment based on studies of the surface-atmosphere exchange of materials in relation to the major biogeochemical cycles and climates [Mooney et al., 1987]. Aside from anthropogenic activities, CO_2 can also be released into the atmosphere naturally. Atmospheric CO_2 can be released through plant and animal decay as microorganisms break down dead material, releasing CO_2

into the air as part of the process. Other naturally occurring sources include forest fires and volcanoes. Just as trees and vegetation are sources of atmospheric CO_2 when they decay, they are also a sink for CO_2 as they grow. During photosynthesis, trees and vegetation absorb CO_2 from the air and emit oxygen. Humans can enhance this carbon sink through reforestation ["The Environmental Literacy Council" 2015].

Atmospheric scientists need a tool to quantify surface energy and turbulent fluxes at the land–atmosphere interface, because these fluxes influence our weather and climate [Pielke et al., 1998]. Baldocchi et al. [2001] reported on such a tool, which consists of a global array of micrometeorological towers that measure turbulent flux densities of CO_2, H_2O, and energy exchange between vegetation and the atmosphere on a continuous and long-term (multiyear) basis. Studies showed that increased concentration of CO_2 in the atmosphere has also increased rate of photosynthesis and plant growth [Drake et al., 1997]. Several micrometeorological methods are used to measure the turbulent fluxes that govern exchanges between the surface and the atmosphere, such as surface energy balance method, bulk transfer method, gradient method, and eddy covariance method.

The surface energy balance method uses an energy balance relationship over a surface and states that the sum of the estimated latent and sensible heat fluxes is equivalent to all other energy sources and sinks:

$$LE + H = Rn - G - S - Q \quad (1)$$

Where LE is the latent heat flux, H is the sensible heat flux, Rn is the net radiation, G is the ground heat flux, S is the rate of change of heat storage between the soil surface and level of instrumentation, and Q is the sum of all additional energy sources and

sinks [*Wilson et al.*, 2002]. The Q term in the equation (1) is typically neglected, resulting in an imbalance between the remaining independently measured parameters in the equation and may cause inaccurate estimates of scalar fluxes such as CO_2, sensible heat, and latent heat. Many studies have been conducted with regard to the energy balance method both on flat and complex terrain; results showed that using the surface energy balance method for flux measurements on complex terrain is not reliable, due to flux footprint and horizontal flux divergence. Flux footprint is simply the surface area contributing to the fluxes being measured. Also, on flat, homogeneous terrain, imbalance in equation (1) is typically present, but minimal [Stannard et al., 1994]. At night, during stable atmospheric conditions, the surface fluxes are usually underestimated; during the daytime, they are overestimated when there is turbulence due to convection.

The bulk transfer method can be used when measurements or computations of mean velocity and temperature are available at just one level, along with the desired surface properties, such as surface roughness and temperature [Arya, 2001]. This method is not reliable because, to use the method, one needs to know the surface roughness, which means surface irregularities and surface temperature; such information is not always easy to come by. For rough and uneven surfaces, the surface itself is not well-defined, therefore the temperature cannot be measured directly.

The gradient method requires one to make measurements at two or more heights in the surface layer. Fluxes are determined from measurements of mean differences or gradients of velocity, temperature, or a scalar between any two heights within the surface layer, but well above roughness elements [Arya, 2001]. While the gradient method is reliable, the eddy covariance method is the most reliable method of making

direct measurements of turbulent exchanges of momentum and heat in the atmosphere.

The eddy covariance method is a micrometeorological technique that gives a direct measure of net scalar, water, momentum, and heat fluxes between vegetated canopies and the atmosphere [Baldocchi, 2003]. This method can measure mass and energy fluxes over short and long timescales (hour, days, seasons, and years) with reduced disturbance to the underlying vegetation and can also sample a relatively large area of land [Baldocchi et al., 2001]. However, this method has some restrictions. The ideal conditions required for the method to work are relatively flat homogeneous terrain, and steady atmospheric conditions [Kaimal and Wyngaard, 1990]. This means the method could present errors if used in complex terrain. However, atmospheric scientists have been conducting eddy covariance studies in non-ideal, complex terrain [e.g., Baldocchi et al., 2000; Geissbühler et al., 2000; Turnipseed et al., 2002; Kominami et al., 2003; Froelich et al., 2005; Froelich and Schmid, 2006]. Eddy covariance measurements in complex terrain might be less problematic over short vegetation compared to tall forests, because a short canopy allows instruments to be located much closer to the surface [Hammerle et al., 2007].

Further research was made by micrometeorologists [Kramm et al., 1995; U et al., 2000; Fuehrer and Friehe, 2002; Massman and Lee, 2002] to revise the theory made by Webb et al [1980] to calculate net exchanges of mass and energy between the surface and the atmosphere, for airflow over non-homogeneous terrain. These micrometeorologists introduced horizontal advection and horizontal mean flux divergence terms in the conservation equation, which made the equation useful for non-steady three-dimensional flow over non-homogeneous terrain. Hong et al. [2008]

investigated the budget equations of H_2O and CO_2 exchanges in a hilly forest catchment. Their field measurements included two eddy-covariance sensors at 20 and 40 m, H_2O, and CO_2 concentration profile on a single tower. Their study was motivated by a general failure of surface energy budget closure and an underestimation of night time respiration (during stable atmospheric conditions) as measured by the eddy covariance method, which is usually as a result of advection, caused by surface heterogeneity and/or low frequency motions [Moncrieff et al., 2004].

Over non-homogeneous terrain, biases in flux observations may result from advection, with different footprints (area contributing to the flux being measured) at different levels [Hong et al., 2008]. Advective effects on carbon exchanges above the canopy using eddy covariance measurements (at different heights on a single tower) were estimated [Yi et al., 2000] and a net ecosystem-atmosphere exchange of CO_2 (NEE) was calculated as the sum of the eddy covariance flux—the rate of change of storage below the eddy covariance measurement. They found that the average difference in total advection between 30m and 122m was as large as 6 μmol m^{-2} s^{-1} during the morning transition from stable to convective conditions and the average difference between 122m and 396m was as large as 4 μmol m^{-2} s^{-1} during daytime [Yi et al., 2000]. Varying flux footprints and pooling of CO_2 in the heterogeneous landscape caused the advection contribution.

In order to quantify surface fluxes in the atmosphere, scientists use MOST (Monin-Obukov Similarity Theory). This theory describes the relationship between the vertical behaviour of dimensionless mean flow and turbulence properties within the atmospheric surface layer (approximately the lowest 10% of the atmospheric

boundary layer) as a function of Monin–Obukov scaling parameters. Obukhov [1946] found a universal-length scale for exchange processes in the atmospheric surface layer, which led to the derivation of the similarity theory by Monin and Obukov in 1954. The Buckingham pi-theorem was used to derive dimensionless wind and temperature profiles [Kantha and Clayson, 2000]. Monin and Obukov found in their study dimensionless groups for the wind and temperature gradient as:

$$\left(\frac{k\,z}{U*}\right)\ \frac{\partial \bar{U}}{\partial z} = \emptyset_m(\zeta) \tag{2}$$

$$\left(\frac{kz}{T*}\right)\frac{\partial \bar{T}}{\partial z} = \emptyset_h(\zeta) \tag{3}$$

$$\mathrm{T}* = \frac{-\overrightarrow{\overline{w'T'}}}{U*} \tag{4}$$

$$\zeta = \frac{z}{L} \tag{5}$$

$$L = -\frac{u_{*T_v}^3}{kg\overline{w'T'}} \tag{6}$$

$\emptyset_m$ and $\emptyset_h$ are the universal similarity constants of momentum and heat flux, k is von karman constant (~0.35), z is the measurement height above the surface, U_* is the friction velocity, $\bar{U}$ is the mean wind speed, $\bar{T}$ is the mean temperature, $\overline{w'T'}$ is the heat flux, T_* is the characteristic dynamical temperature, g is acceleration due to gravity (~10m/s), and L is the Monin-Obukov length.

Monin and Obukov [1954] showed that in the case of thermally stratified atmosphere, wind and temperature profiles must be functions of ζ in equation (5), which is a dimensionless stability parameter because they determine the stability conditions of the atmosphere. Many scientists have worked towards determining universal functions as functions of atmospheric stability [Swinbank, 1968, Dyer and Hicks, 1970]. Their research was focused on the atmospheric surface layer (~lowest few tens of metres above the surface); they found that fluxes of heat and momentum

are constant within the surface layer under unstable atmospheric conditions. The universal functions used in the work of Businger et al [1971] were based on the observations from the 1968 Kansas field experiment and are widely used in micrometeorological experiments and modelling. MOST has been tested and used on flat, homogeneous terrain. Research has shown an agreement between profile-derived and measured surface fluxes over an entire stability range of observations on horizontally uniform, flat terrain [Businger et al., 1971].

There are limitations to the use of MOST, one of which is the roughness sub-layer, usually above the canopy and up to 2-3 times the canopy height [Foken, 2006]. These effects cannot be neglected for vegetated surfaces with canopy height greater than 0.1m [Raupach et al., 1980]. Therefore, in such cases, the profile equations need to be modified using a universal function that depends on the height of the roughness sub-layer [Garratt et al. 1992]. The universal functions are also prone to errors when there is non-closure of energy balance, which is caused by underestimation of turbulent fluxes measured while temperature and wind gradients are exactly measured [Foken, 2006]. MOST is restricted to the surface layer above the roughness sub-layer and over homogeneous surfaces; discrepancies may occur if applied to complex terrain and above tall vegetation. Generally, MOST was used in our research to estimate the Monin-Obukov stability parameter, friction velocity (momentum flux), and log wind profile.

Strongly stable atmospheric conditions usually lead to cold air pools in complex terrain. Many studies have been conducted on cold air pools in complex terrains [Whiteman, 1982; Mahrt et al., 2001; Lareau et al., 2012; Mahrt and Heald, 2014]. Cold air pools (CAPs) occur when atmospheric processes allow the cooling of air near the surface and warming aloft, which leads to cold air settling at the bottom of

a valley. A temperature inversion, which is an increase in temperature with height, is an atmospheric phenomenon that initiates a cold air pool. The major types of temperature inversions are surface and subsidence inversions. Surface inversion is a diurnal type of inversion that occurs at night during calm or weak winds with colder air at the Earth's surface due to radiative cooling and warmer air above. This type of inversion could persist for days or weeks during winter season because surface radiative heating at daytime is not sufficient to completely destroy CAP during winter periods [Zhong et al., 2001]. A subsidence inversion develops when the temperature increases with height in the upper atmosphere due to large mass of air sinking from the upper level, which warms adiabatically. If the air mass sinks low enough, it will allow warmer air above and colder air below, which is common in mountainous regions during high pressure synoptic conditions.

Understanding the interactions between winds above (synoptic flow) and within a valley (local flow) helps in predicting the dispersion of pollutants that are either released at ground level or elevated level [Whiteman and Doran, 1993]. Sometimes pollutants transported from another region could remain aloft and not mix down to the surface, which could be due to weak winds not being able to mix down air from above to the surface. Geiss et.al [2015] deployed a sonic anemometer at 20 m and 1m on a tower placed in a small valley, to investigate local nocturnal circulations. They compared the correlation between wind direction at heights of 20 m and 1m with reference to the valley. When the winds at the height of 20 m is uncorrelated with those at the height 1 m and the winds at 1 m is in agreement with that in the valley, then the event is associated with cold pool in the valley, which is the period of weak winds and strong temperature inversion [Geiss and Mahrt, 2015].

Topography influences CAPs. Many studies have investigated CAP in deep valleys, steep slopes, and shallow valleys, which found that wide, shallow valleys are more prone to external atmospheric influence because they are less sheltered by topography [Barr and Orgill, 1989; Banta et al., 1995; Papadopoulos and Helmis, 1999; Mahrt et al., 2001; Mahrt and Heald, 2014].

CAPs impact air quality because they trap pollutants within the boundary layer raising pollutant concentrations to unhealthy levels. Studies have shown that pollutants increase in concentration during CAP periods, even after terminating their release [Allwine et al., 1992; Silcox et al., 2012]. This is one of the reasons why the western part of United States (mountainous region) are struggling to meet the National Ambient Air Quality Standards (NAAQS), because of the complex terrain, which favors persistent CAP formation. This is also an issue to air quality scientists because models such as the Weather Research and Forecasting Model (WRF) and Fifth-Generation NCAR/Penn State Mesoscale Model (MM5), usually underestimate atmospheric conditions that lead to elevated $PM_{2.5}$ concentrations during persistent cold air pool [Baker et al., 2011].

Most air quality studies focus on urban areas because of pollutant emissions from industries, power plants, and vehicles in cities [Grimmond et al., 2002; Contini et al., 2012]. Grimmond et al. [2002] showed that urban surface is always a net source of CO_2, even the presence of vegetation would not offset the significant anthropogenic sources. Atmospheric stability also influences the fluxes of CO_2. This was shown in the study of Goulden et al. [1996]. The fluxes of CO_2 increased in winter during windy periods because winds forced the CO_2 out of the soil and snow pore space.

1.2 Overview of the Research

The properties of the atmospheric surface layer are different in rolling terrain when compared to that of flat terrain with implications on surface fluxes. Over flat, homogeneous terrain, the logarithmic dependence of wind speed with height (referred to hereafter as the log law) is often used to model wind speed in the neutrally stratified surface layer. The underlying surface properties considered are, roughness, canopy height, and other obstacles. The log law will be investigated in this research to see if the log-wind profile fits the wind speed as the study site used in this research is a rolling terrain, which violates one of the assumptions required for the log law to be valid.

The surface flux measuring tower was placed in a shallow valley to isolate CAP event during night-time stable atmospheric boundary layer, and to investigate its impact on surface fluxes of heat, moisture, and CO_2. An irrigated farmland is located near the study site and this is expected to impact the latent heat (moisture) flux. Evaporation of moisture into the atmosphere impacts the weather as more water vapour condenses to form cloud water droplet during daytime convective activities.

This study is intended to demonstrate the influence of temperature inversions and atmospheric turbulence on the fluxes of heat, moisture, and CO_2 in a rural region on rolling terrain. The results can be compared with that of Weather Research and Forecasting model (WRF) to evaluate it as most models break down on complex or rolling terrain especially during very stable atmospheric conditions. This is important for air-pollution monitoring on complex terrain because it is strongly influenced by divergence and convergence, as pollutants accumulate in the valley at nighttime due to surface based temperature inversion, and during daytime mixing occurs as the inversion layer erodes due to incidence solar radiation.

Chapter 2: Methods

2.1 Site Description

The field experiment was conducted near Echo, Oregon for a period of 1 week in September 2014. The city of Echo is situated near the Umatilla River within a tree-lined valley known as the Echo Meadows in the Columbia River Basin. The elevation of the city is ~194.5m and has a semi-arid climate. It is a rural area located at 45.713560^{o} N, 119.406023^{o} W. The mean monthly high is ~74^{o} F and the mean monthly low is approximately 41^{o} F. The hottest month is July while the coldest month is January. The landscape of the measurement site is dominated by center pivot irrigated farmland with the presence of over 100 wind turbines. The surface is covered with short grass on rolling terrain. A photograph of the measurement site shows the surface flux tower and instruments in Figure 2.1 and 2.2.

A 10 m flux tower was installed in a small valley depression to isolate night time cold air pooling. Two IRGASON and two EC150/CSAT3 (Campbell Scientific Inc., Utah) were mounted on the tower at four heights. The measurement site did not have access to a power supply, so a generator was used to power the instruments and collect data. There were days when the generator stopped working, and this was reflected as gaps in the plots presented in the results and discussion section.

Figure 2.1. Photograph of the measurement site showing the rolling terrain and an irrigated farmland nearby. [Photograph taken by Jason Kelley, 2014].

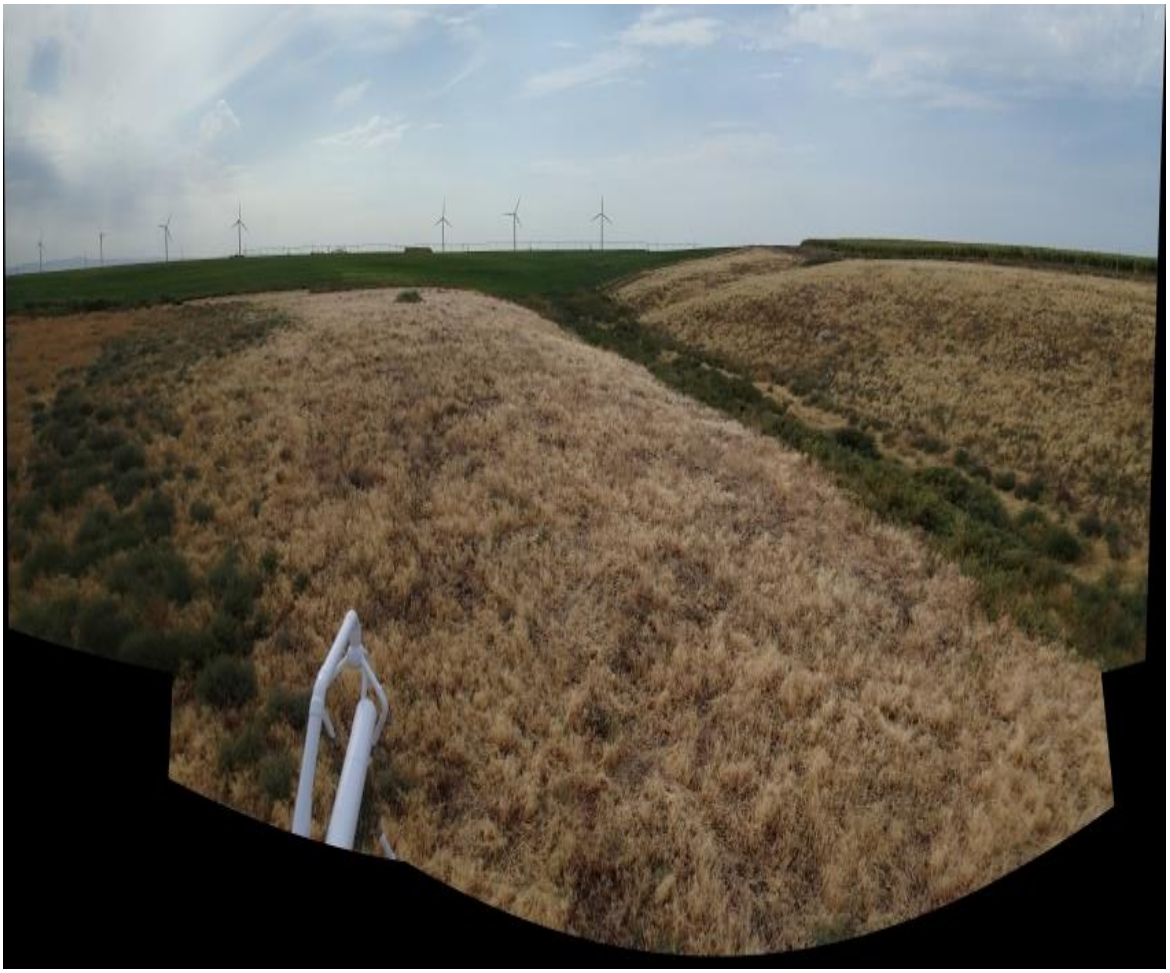

Figure 2.2. Photograph of the site terrain looking into the prevailing wind. [Photograph taken by Jason Kelley, 2014].

2.2 Surface Flux Data

2.2.1 Measurement Data

The instantaneous wind speed and temperature data were collected at 1.1m, 2.7m, 4.8m and 7.7m above the ground using 3D sonic anemometers (Campbell Scientific, CSAT3, see Fig. 2.3) at a sampling frequency of 10 Hz. The sampling

frequency (10 Hz) was used to allow smaller eddies to be captured during the measurement. Eddies are defined here as winds generated near the earth's surface that grow bigger in size with height above the ground during convection at daytime. The sonic anemometers were aligned in the direction facing the prevailing wind at an angle of 221^{o}. This was done based on the direction of wind at the measurement site to reduce flow distortion around the sonic anemometer most of the time. Sonic virtual temperature (T_s) was also collected from the sonic anemometer, but it is not the same as virtual potential temperature (Θ_v) because it was calculated using a constant pressure. Although, sonic virtual temperature is not equal to virtual potential temperature, it is still a good approximation in dry atmospheric conditions [Metzger and Holmes, 2007]. An open path infra-red gas analyser (see Fig. 2.4) was used to collect CO_2 and H_2O concentrations at four heights as stated above at the same sampling frequency as the sonic anemometer (10 HZ).

Figure 2.3. Photograph of the CSAT3 sonic anemometer. [Image Reference: https://www.campbellsci.com/irgason].

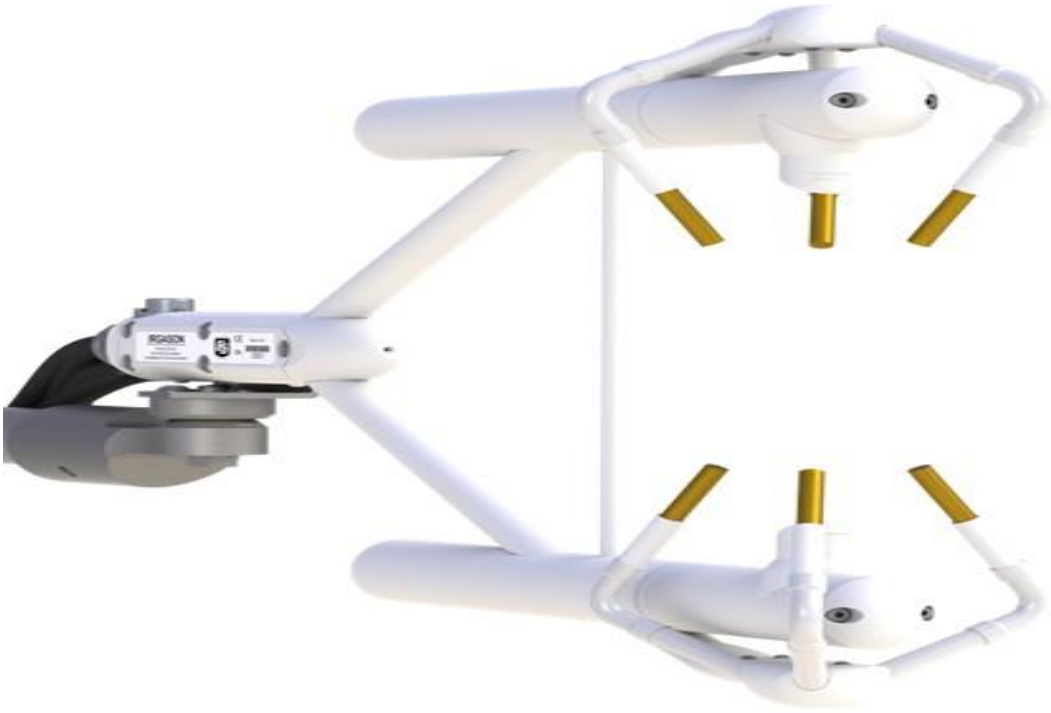

Figure 2.4. Photograph of the IRGASON open path infrared gas analyser. [Image Reference: https://www.campbellsci.com/irgason].

2.2.2 Reynolds Decomposition

There are several methods of separating turbulence from mesoscale motions in time series micrometeorological data, such as block averaging, polyfitting (linear detrend), cospectra or spectra gap time scale, multi-resolution flux decomposition and much more. Researchers have worked on turbulent flux calculations using different time scales for mean removal [Howell and Sun, 1999; Vickers and Mahrt, 2003, 2005]. In our study, polyfitting linear detrend was used to separate turbulent scales of motion from that of the mesoscale. The raw data was analysed using 5 minutes, 15 minutes, and 30 minutes linear detrend and all turbulent fluxes were calculated using a 30 minute average.

The 30 minute averaging time is recommended because it is assumed that atmospheric processes are stationary within this period, where 10-20 minute is usually required for daytime unstable atmosphere and about 30-60 minute (sometimes as high as 120 minute) is required for nighttime stable atmosphere. However, no remarkable error would occur if 30 minute is used over the whole day [Foken, 2008]. Linear detrending the data removes perturbations from the mean according to the rules of Reynolds decomposition. Reynolds decomposition is a mathematical method used to separate the average and fluctuating parts of a quantity. An example of Reynolds decomposition for zonal wind speed (u) is given as:

$$u = \bar{u} + u' \tag{7}$$

Where $\bar{u}$ denotes the time average of u, and u' is the fluctuating part (perturbations). In this work, three different time scales (5 minutes, 15 minutes and 30 minutes) were used for Reynolds decomposition to see if there is a significant difference between shorter and longer time scales on the calculated fluxes. In the process of removing the turbulent motions from the mesoscale motions using a longer time scale under stable atmospheric conditions, mesoscale motions could be accidentally added to the turbulent flow, and this is problematic when computing the fluxes [Howell and Sun, 1999; Vickers and Mahrt, 2003]. It was observed that momentum flux increases slightly with increasing averaging time for mean removal [Vickers and Mahrt, 2003]. If shorter sampling times are used, low frequency contributions to the fluxes are missed, and the steady state condition may not be met for longer time scales [Moncrieff et al., 2004; Foken, 2008].

2.2.3 Co-ordinate Rotation and Planar fit

The Wilckzak planar fit method is used to correct sonic tilt which could be a source of error on calculated surface fluxes especially on complex or sloping terrain [Wilczak et al., 2001]. This is important because some of the horizontal wind component could be accidentally read in the vertical due to sonic tilt. This is common on terrain that is not flat. Planar fit could also be done on flat terrain because a period of strong winds could also tilt the sonic anemometer from its aligned position. Also, researchers using eddy covariance measurements to estimate scalar surface fluxes such as CO_2 and H_2O on complex or rolling terrain need to use planar fit method to remove the vertical mean velocities. The planar fit method forces the mean vertical velocities to zero for each averaging period. The Planar fit method was adopted in our research because the study site is rolling terrain, and a tilt in the sonic anemometers would give erroneous vertical wind data. If there were no vertical wind data collected, planar fit would not have been necessary. More details can be seen in Wilczak [et al., 2001].

2.3 Surface Flux Calculations

Surface flux calculations are done based on 30-60 minutes averaging because it is usually assumed that atmospheric processes are stationary within this period [Foken, 2008]. The surface flux calculations were done by eddy covariance method and the atmospheric stability parameter was calculated according to Obukov [1946]. The friction velocity u_* was calculated using momentum flux;

$$u_* = (\overline{u'w'}^2 + \overline{v'w'}^2)^{1/4}. \quad (8)$$

Friction velocity is a measure of turbulence; it shows how strong Reynolds stresses are on a flow. The water vapor collected by an open path infrared gas analyser (IRGA) was used to calculate latent heat flux:

$$F_E = L_v \overline{w'q'} \ . \quad (9)$$

Where L_v is the latent heat of vaporization of water (J kg^{-1}), $\overline{w'q'}$ is the covariance of the vertical wind speed and moisture. The sensible heat flux is given as:

$$F_H = \rho C_p \overline{w'T'} \ . \quad (10)$$

C_p is the specific heat capacity at constant pressure (J $kg^{-1}K^{-1}$), ρ is air density (~1.01kg m^{-3}), $\overline{w'T'}$ is the covariance of vertical wind speed and temperature. CO_2 flux was calculated as:

$$F_C = \rho \overline{w'C'} \ . \quad (11)$$

The overbar represents the Reynolds average and the prime represents the turbulent fluctuations from this average. C represents a scalar, which in this case, is CO_2 (ppm). ρ is the air density (kg m^{-3}). The Monin-Obukov Length was calculated as the ratio of mechanical to buoyancy forces and is given as:

$$L = \frac{-u_*^3 \overline{\theta_v}}{k\, g\, (\overline{w'\theta'_v})} \ . \quad (12)$$

Where k is von Karman constant empirically determined to be 0.4 and g is acceleration due gravity (m/s^2). Θ_v is the virtual potential temperature assumed to be approximated by the sonic temperature (T_s). The Monin-Obukov length can be used to determine stability. However, a widely used stability parameter is the

dimensionless Monin-Obukov length, which is defined as:

$$\zeta = \frac{z}{L} \tag{13}$$

Here z is the measurement height and L is the Monin-Obukov length defined in Equation (9). Stability classification for the dimensionless stability parameter is:

$\frac{z}{L} < 0$ unstable atmospheric condition (14)

$\frac{z}{L} = 0$ neutral atmospheric condition (15)

$\frac{z}{L} > 0$ stable atmospheric condition (16)

In this study, we used dimensionless Monin-Obukov stability parameter to determine the stability conditions of the atmosphere. The temperature gradient was also calculated to determine when there was a temperature inversion, which can also be used as an estimate of stability. A temperature inversion is defined as an increase in temperature with height. Four measurement heights were used in this study; therefore, the temperature gradient was calculated between the upper level sensor (7.7m) and lowest level sensor (1.1m) as:

$$\frac{\Delta T}{\Delta Z} = \frac{T_4 - T_1}{z_4 - z_1} \tag{17}$$

T_4 represents the temperature at sensor height 7.7m, T_1 is the temperature at sensor height 1.1m, z_4 and z_1 are the sensor heights respectively. A positive temperature gradient signifies a temperature inversion, which usually occurs at night or during stable atmospheric conditions. A negative temperature gradient is common during daytime, signifying convection or unstable atmospheric conditions depending on the comparison with the dry adiabatic lapse rate.

Atmospheric stability influences surface fluxes; this has drawn the attention of scientists because pollutants are increased to higher levels during stable atmospheric

conditions within the boundary layer. The fluxes of CO_2 are usually underestimated at night (during calm stable atmospheric condition) and overestimated at daytime (during unstable atmospheric condition). There is a correlation between CO_2 flux and u_*. Research has shown that turbulence affects the movement of CO_2 out of the soil during windy conditions, where CO_2 flux increased during windy periods ($u_* > 0.8$ ms^{-1}) in winter [Goulden et al., 1996].

2.4 Logarithmic Wind Profile

Studying the nature of the wind profile within the surface layer is important because it determines the structure of surface roughness elements such as, buildings, bridges, pollutant dispersion, and wind turbines. The log law is an empirical way to couple the surface with the atmosphere in terms of wind. It can also be used to estimate roughness length (z_o). Under neutrally stratified conditions, wind speed varies approximately logarithmically with height in the surface layer, which has been shown by many scientists [Stull, 1988; Foken, 2008]. Near the ground surface, wind speed becomes zero due to frictional drag, while wind speed increases with height due to pressure gradient force. The log law is well-known for wind speed in the neutrally stratified surface layer over flat, homogeneous terrain and has been studied in wind tunnels and pipes. This law is only valid based on some assumptions such as, neutral atmospheric conditions, flat terrain, homogeneous surface (constant surface roughness), and steady wind speed. In a neutral boundary layer, only the mechanical turbulence dominates, which is associated with wind shear and surface stress [Stull, 1988]. The study site used in our research is rolling terrain, which undermines one of the assumptions required for log law to hold.

The logarithmic (log) wind profile relationship can be determined using the Buckingham Pi Theory to derive two dimensionless groups, which are $\frac{\bar{U}}{u_*}$ and $\frac{z}{z_o}$. Then, the log wind profile equation is given as:

$$\frac{\bar{U}}{u_*} = \left(\frac{1}{k}\right) \ln\left(\frac{z}{z_o}\right) \quad . \tag{18}$$

Here $\bar{U}$ is the mean wind speed, u_* is the friction velocity, k is von Karman constant (0.4), z is the measurement height above the ground surface, and z_o is the aerodynamic roughness length.

Chapter 3: Results

3.1 Mean Meteorological Variables

Temperature (T), wind speed (WS), wind direction (WD), CO_2, and H_2O concentrations were averaged to 30-minutes to determine diurnal variations during one week in September at the measurement site. Temperature gradient was also calculated between the top and bottom sensor (7.7m-1.1m) and averaged over 30-minutes to determine periods associated with temperature inversions. This is true at night when cold air settles on the slight valley depression where the bottom sensor was mounted. Figures 3.1-3.5 show the diurnal pattern of these variables (T, Temp. gradient, WS, WD, and CO_2) at the measurement site, which are expected to portray strong diurnal variation because the site is semi-arid and consists of dry short grass.

Convective mixing is evident at daytime, which makes nearly uniform temperature as seen in Figure 3.1 where the temperature at each height is almost the same during daytime. Increase in temperature with height was observed during nighttime. Figure 3.2 shows the temperature gradient calculated between the top sensor (7.7m) and the bottom sensor (1.1m). This plot illustrates the diurnal atmospheric stability and instability in terms of the positive and negative temperature gradient. A positive temperature gradient denotes a period of stable atmospheric conditions, which is associated with weak winds and temperature inversion. A negative temperature gradient denotes a period of atmospheric instability, which is associated with strong winds and a decrease in temperature with height. The most interesting day is on the night of 26 September 2014. The strongest temperature inversion was observed on this day ($\sim+1^{\circ}K\ m^{-1}$) compared to other days in the data. Researchers at the site reported that the cold air pool was felt at the bottom of the

measurement tower in the depression, and there was warm air on the road at the top of the small valley depression.

An increase in wind speed with height (wind gradient) is known as wind shear. The process by which heat and other atmospheric properties mix due to wind shear is known as forced convection. Forced convection is also called mechanical turbulence, which is generated when winds blow over obstructions like mountains and buildings at the surface. This type of turbulence is common in complex terrain. Turbulence can also be generated during daytime due to surface heating when solar radiation heats the Earth's surface, convective or thermal turbulence. Figure 3.3 shows the diurnal wind speed pattern, which increased with height on all days. The highest wind speed (~5.8 m s^{-1}) was observed during daytime on 24 September 2014, and this was a dark, cloudy, stormy day at the measurement site. Strong transition was observed in the wind speeds from night time to daytime due to the transitioning of the boundary layer at sunrise from the nocturnal boundary layer to the daytime convective boundary layer.

Figure 3.4 shows the diurnal wind direction pattern, which on average was south-westerly except for a few days in the data that showed a north-easterly wind direction. The observed south-westerly winds in the data correlate with the stormy, cloudy days that brought rain to the measurement site because south-westerly winds are associated with moisture since the measuring sensors used in this study were aligned at an angle 221^{o}, which lies in the south-west wind direction.

Moisture generally decrease with height, which means that the surface is the source of moisture. However, the water vapour concentration in Figure 3.5 shows that there was an increase in moisture with height. This is likely due to a horizontal advection of

moisture from the irrigated farmland near our study site. The implication of this on the moisture (latent) flux will be discussed in the next section.

During the daytime period, plants are actively undergoing the process of photosynthesis, so CO_2 is being removed from the atmosphere near the surface. Strong winds cause mixing in CO_2 and facilitate their release to plants for the process of photosynthesis. However, weak winds allow the concentration of CO_2 to accumulate within the boundary layer. Figure 3.6 depicts the diurnal pattern of the CO_2 concentration, which was observed to decrease with height except for a few cases, where there was mixing in the concentration during the daytime period. The most interesting day in the data had the highest concentration of CO_2 (~485 ppm), which correlates with the strongest temperature inversion observed on the same day at nighttime.

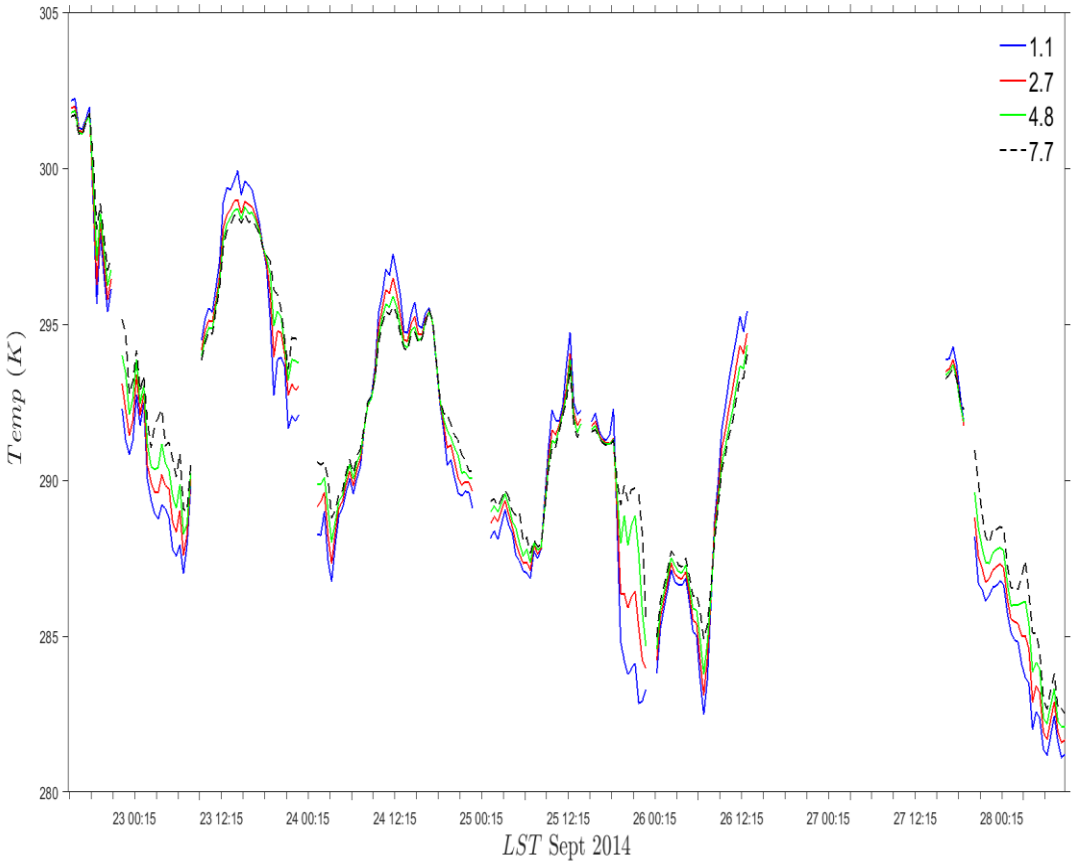

Figure 3.1. Diurnal temperature pattern from the IRGASON open path gas analyser located in Echo, Oregon from 22 September 2014 through 28 September 2014. The manufacturer quotes $\pm$ 0.1 uncertainty for this temperature range.

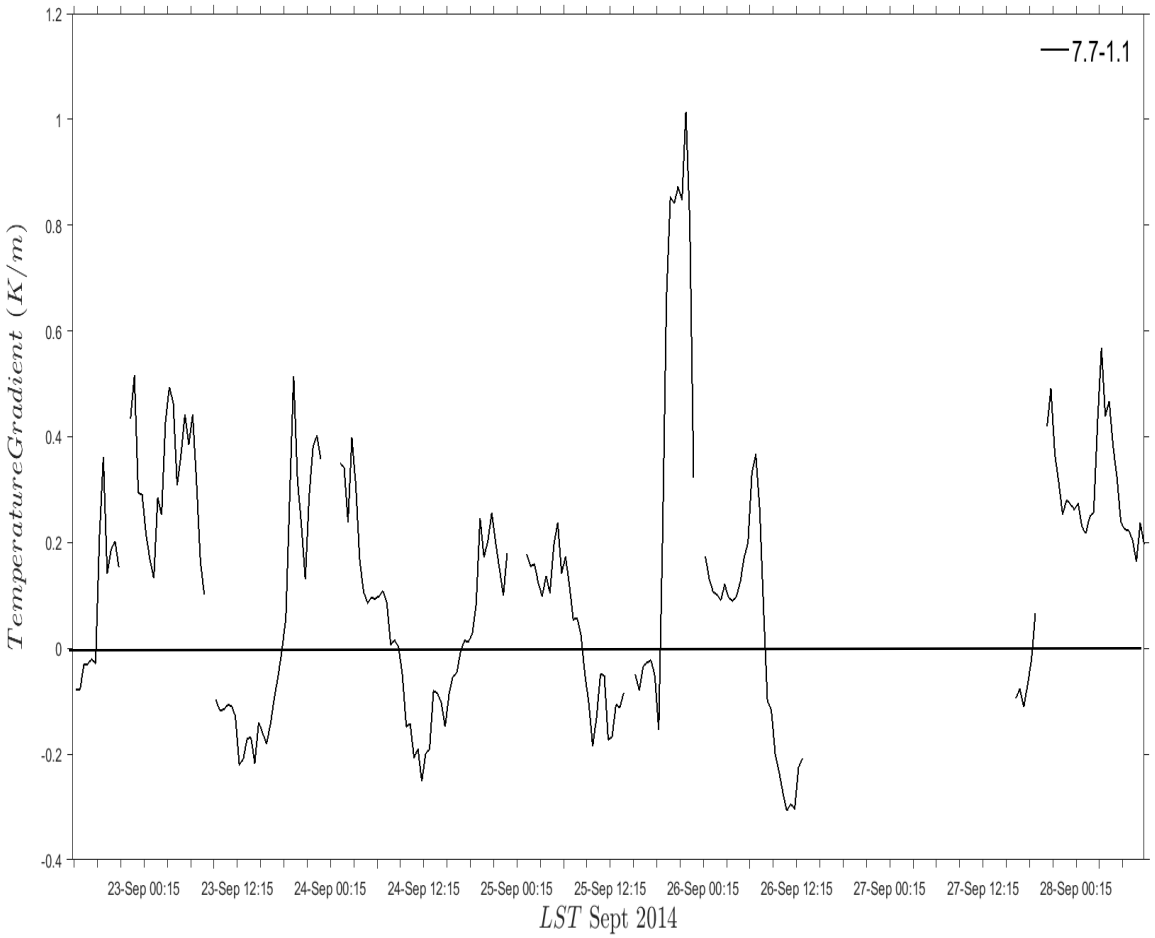

Figure 3.2. Diurnal temperature gradient pattern calculated between height 7.7m and 1.1m at Echo, Oregon from 22 September 2014 through 28 September 2014.

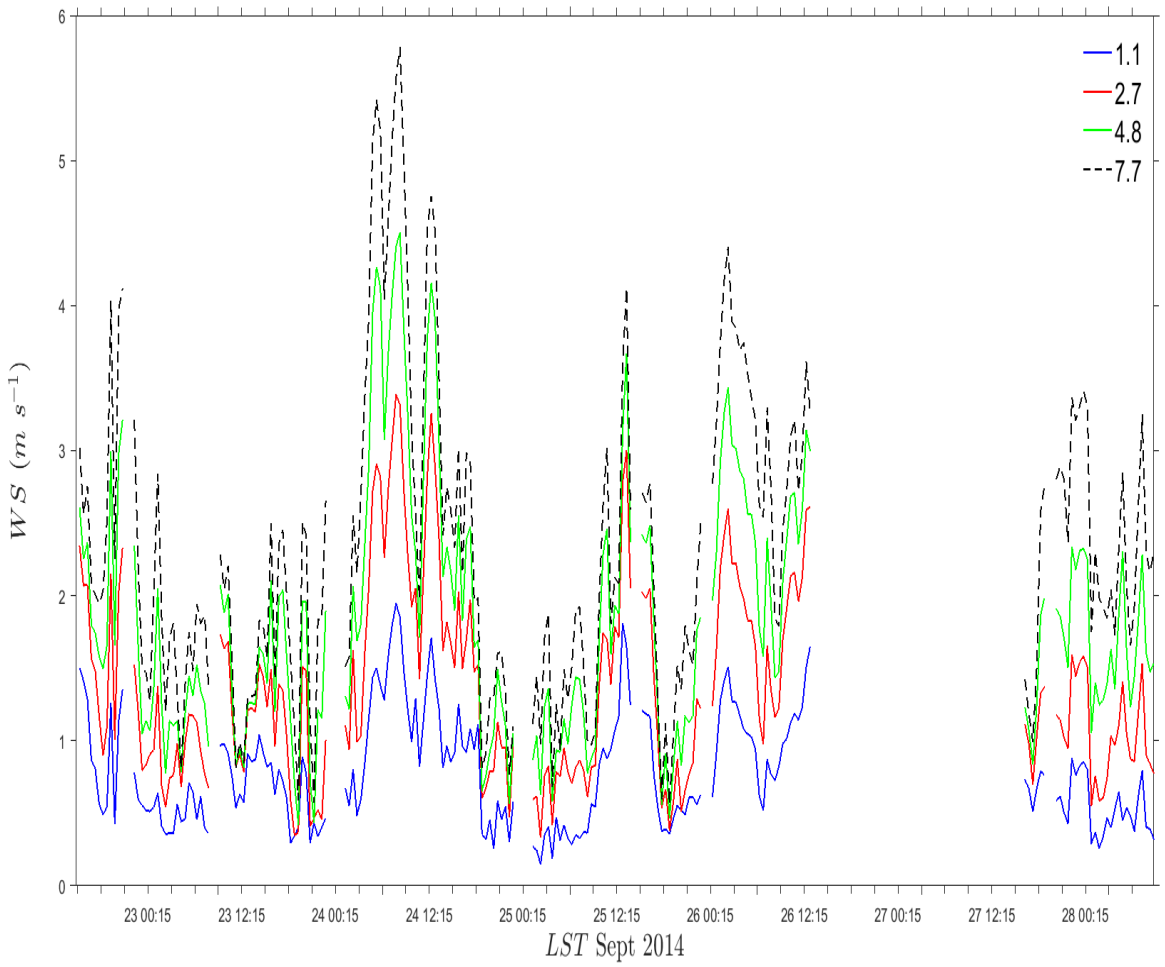

Figure 3.3. 30 minute time series wind speed at four heights 1.1m, 2.7m, 4.8m, and 7.7m at Echo, Oregon from 22 September 2014 through 28 September 2014.

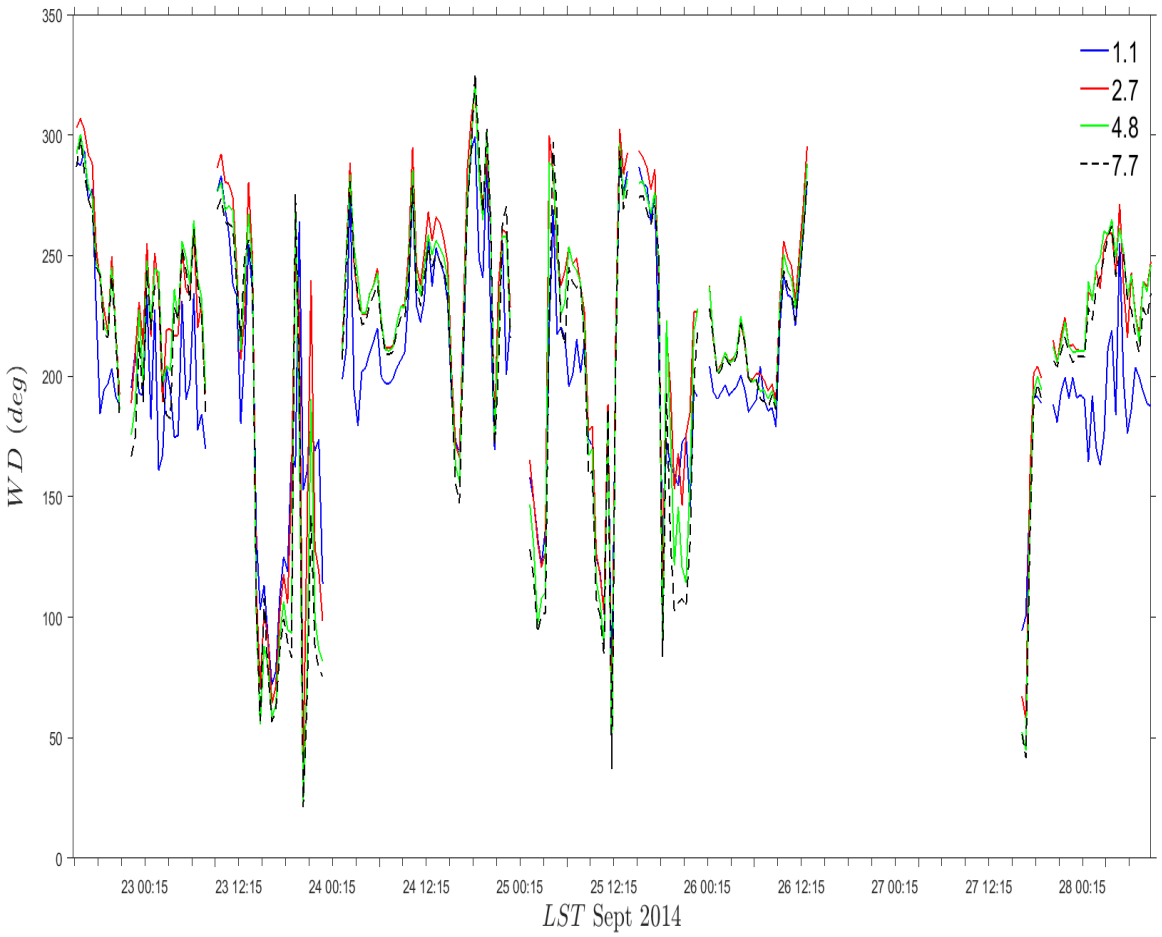

Figure 3.4. 30 minute diurnal wind direction at four heights 1.1m, 2.7m, 4.8m, and 7.7m at Echo, Oregon from 22 September 2014 through 28 September 2014.

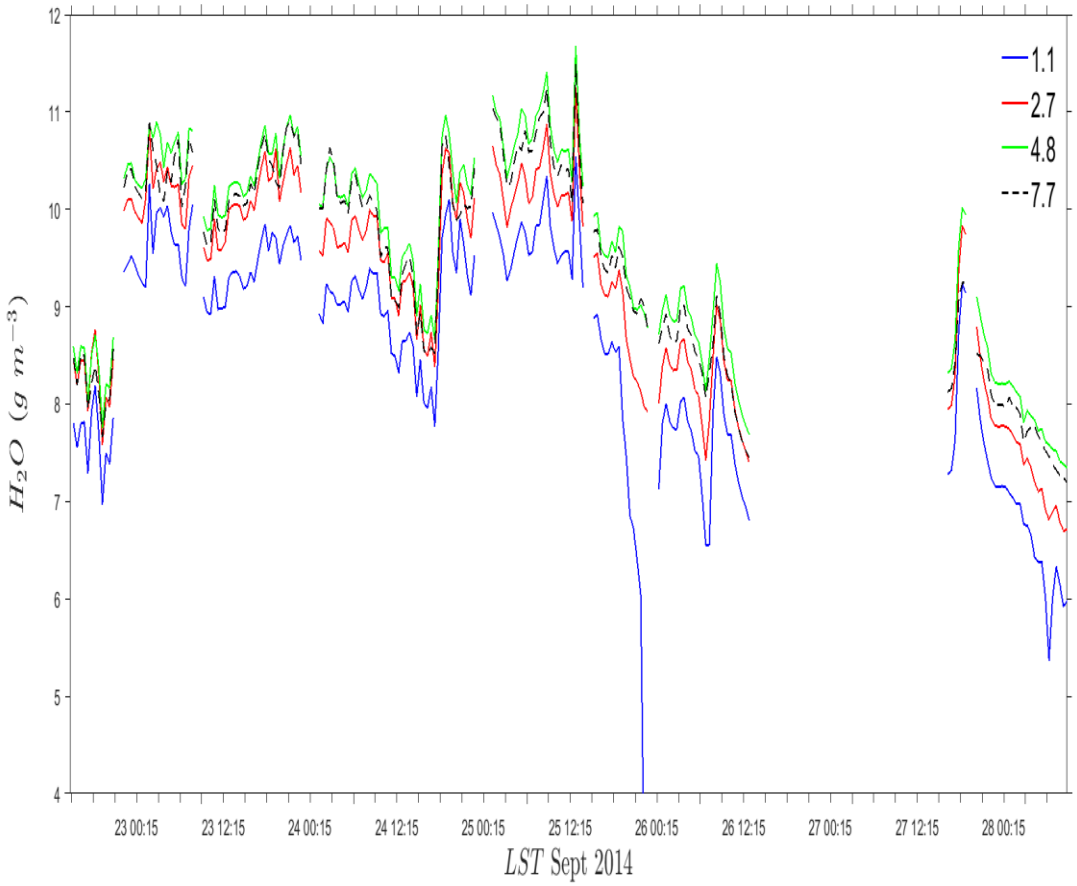

Figure 3.5. Diurnal variation of water vapour concentration at four measurement heights 1.1m, 2.7m, 4.8m, and 7.7m at Echo, Oregon from 22 September 2014 through 28 September 2014.

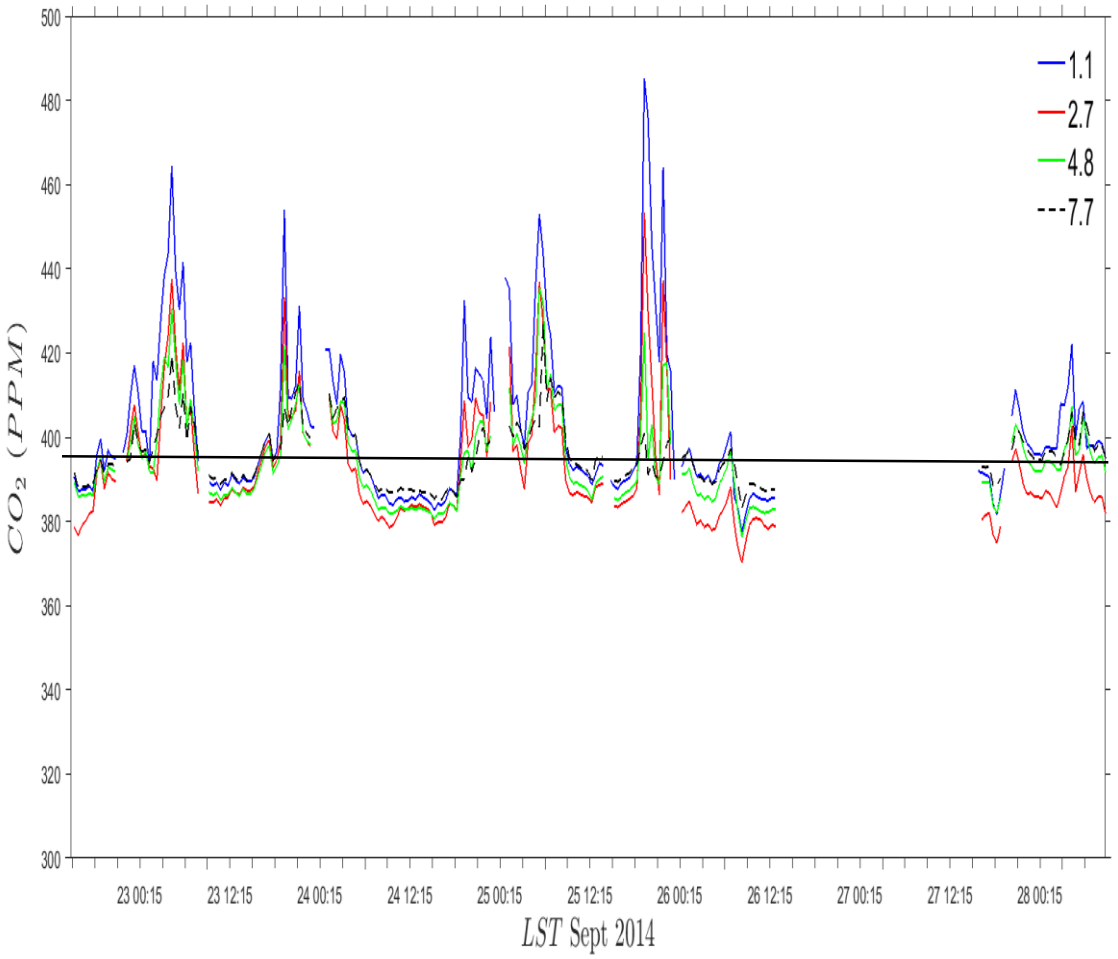

Figure 3.6. 30 minute time series CO_2 concentration (ppm) at four heights 1.1m, 2.7m, 4.8m, and 7.7m at Echo, Oregon from 22 September 2014 through 28 September 2014. The black line represents 2013 global average CO_2 concentration ~395ppm based on the work of Dr. Pieter Tans [esrl.noaa.gov].

3.2 Surface Fluxes at Four Heights

Surface fluxes of sensible heat, latent heat, momentum and CO_2 were calculated based on a 30-minute averaging. 3 different time scales (5-minutes, 15-

minutes, and 30-minutes) were used to remove the turbulent motions from the synoptic motions to see if there would be a significant change in the fluxes at different time scales. A 15-minute mean-removal time scale was chosen in this research because of the evolution period of the boundary layer as discovered by previous researchers. Boundary layer stationarity is assumed within 15-minute intervals during daytime period, and that is one of the reasons why most micrometeorologists prefer 15-minute linear detrend [Pattey et al., 2006]. Longer mean-removal time scales may be required at night time to account for intermittent/irregular turbulence [Massman and Lee, 2002]. Figures 3.7a-3.10 show the diurnal variation of the surface fluxes calculated using the methods described in the previous section.

The diurnal pattern of sensible heat flux is presented in Figure 3.7a, which showed positive flux (upward flux) during daytime and negative flux (downward flux) at night time. This observation is reasonable because solar radiation is transmitted to the surface at daytime, and the surface emits heat in form of sensible heat and latent heat. Long wave radiation is always emitted by the surface and atmosphere. Cloudy skies result in more downwelling infrared radiation at the surface than clear skies. On a clear day the surface cools at night strongly since it emits a lot of infrared radiation, yet doesn't receive so much back from the atmosphere. The sensible heat flux was almost zero on the night of 25 September 2014 unlike other days in the data, which seems unique, and the maximum upward flux (~200 W m^{-2}) was observed on 26 September 2014 during daytime. Variability in the sensible heat flux was estimated by calculating the standard deviation and average values of the data, which is presented in Figure 3.7b. Under the most stable conditions,

variability is closer to minimum. Thus, it is assumed as an uncertainty in the measurement (~± 5 W m^{-2}).

Figure 3.8 presents the latent heat flux, which showed similar diurnal variation with that of sensible heat flux. The latent heat flux increased with height, which means the surface under the measuring sensor was probably not the source of moisture, so it could have been transported (horizontal advection) from the irrigated farmland near the measurement site. Moisture gradient was observed in the water vapour concentration presented in Figure 3.5. Maximum upward flux of the latent heat (~118 Wm^{-2}) was observed on 24 September 2014 during daytime, which was the day it rained on the measurement site and the farm nearby was irrigated.

Micrometeorologists consider friction velocity as the measure of atmospheric turbulence because of the cross wind components in Equation (8), which is a measure of momentum and it can be used to filter bad data points obtained during very weak turbulence when friction velocity is very low. Surface roughness also impacts friction velocity. Surface roughness refers to the surface texture, the elements present at the surface such as trees and grasses. Surface roughness is difficult to determine in complex terrain due to non-uniformity in surface properties. Figure 3.9 show the diurnal pattern of the friction velocity, which is a measure of momentum flux. Strong diurnal variation was observed in the friction velocity as the daytime values were higher and nighttime values were lower. The maximum friction velocity (~0.67 ms^{-1}) was observed on 25 September 2014 at daytime.

The flux of CO_2 was negative (downward flux) during the daytime and positive at nighttime (upward flux) in Figure 3.10. The downward flux of CO_2 was

lowest (~ -0.8 mg $m^{-2}s^{-1}$) on 26 September 2014 during the daytime period. This correlates to the same time the sensible heat flux was at its maximum in the data, which signifies a strong solar radiation incidence at the surface generating strong winds (convective or thermal turbulence) that results in maximum depletion in CO_2.

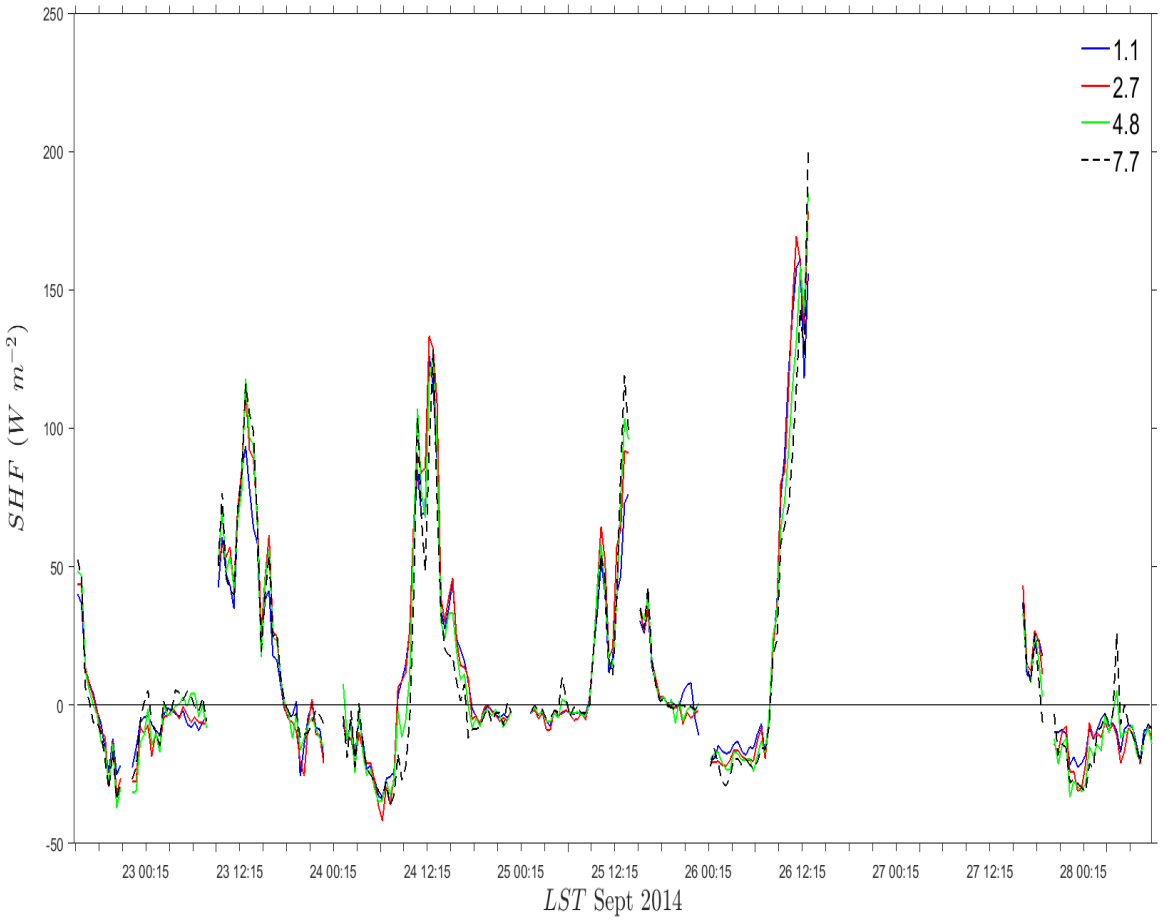

Figure 3.7a. Diurnal variation of sensible heat flux at four measurement heights 1.1m, 2.7m, 4.8m, and 7.7m at Echo, Oregon from 22 September 2014 through 28 September 2014.

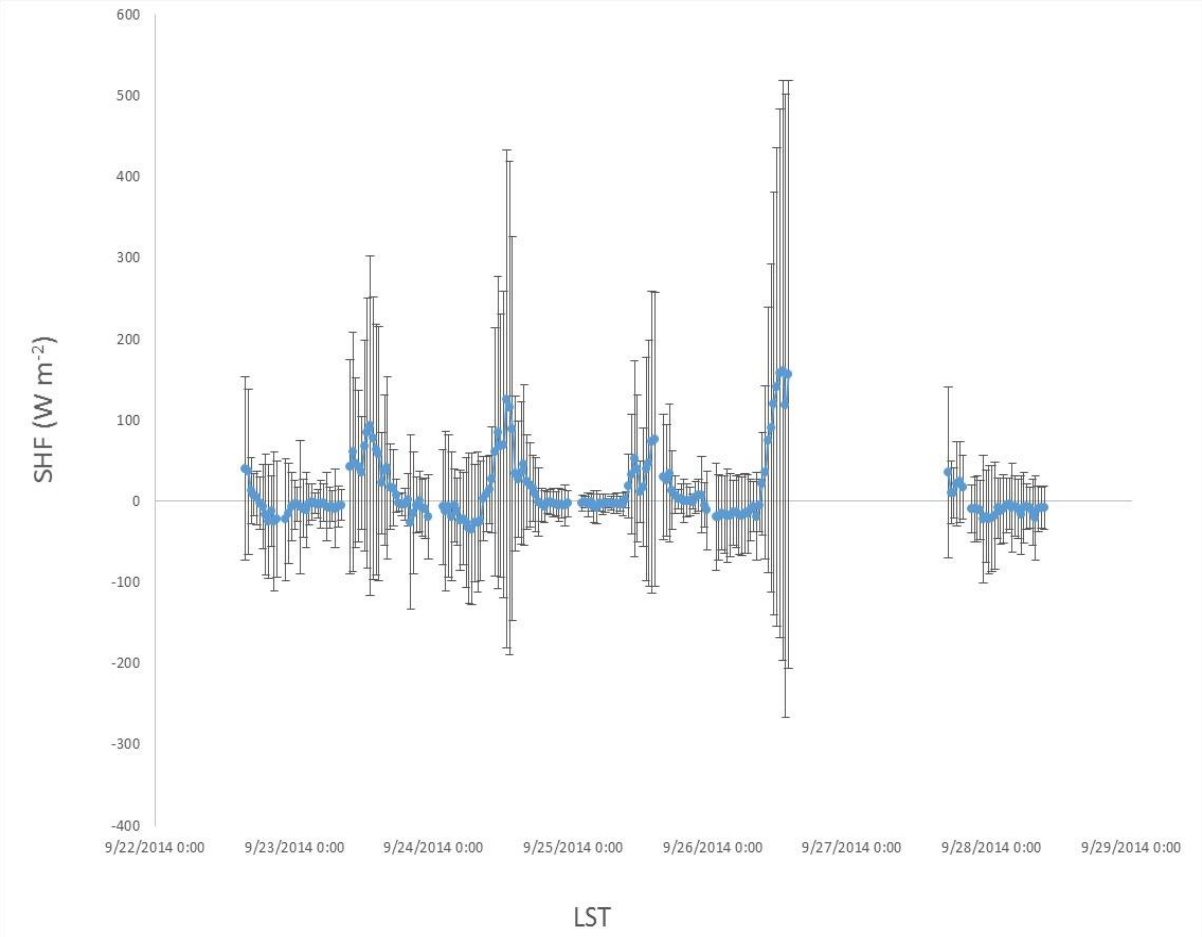

Figure 3.7b. Standard deviation of the diurnal variation of sensible heat flux as a measure of variability.

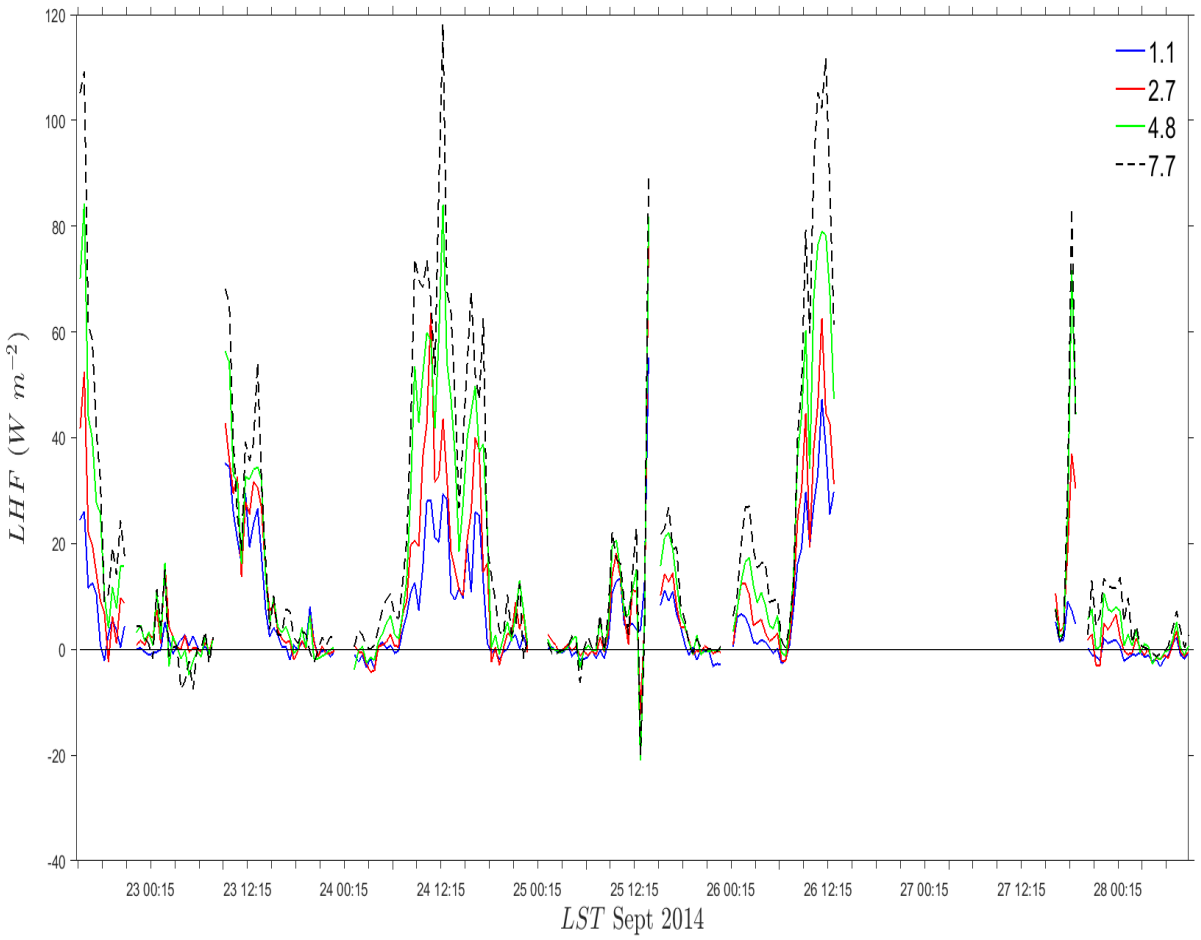

Figure 3.8. Diurnal variation of latent heat flux at four measurement heights 1.1m, 2.7m, 4.8m, and 7.7m at Echo, Oregon from 22 September 2014 through 28 September 2014.

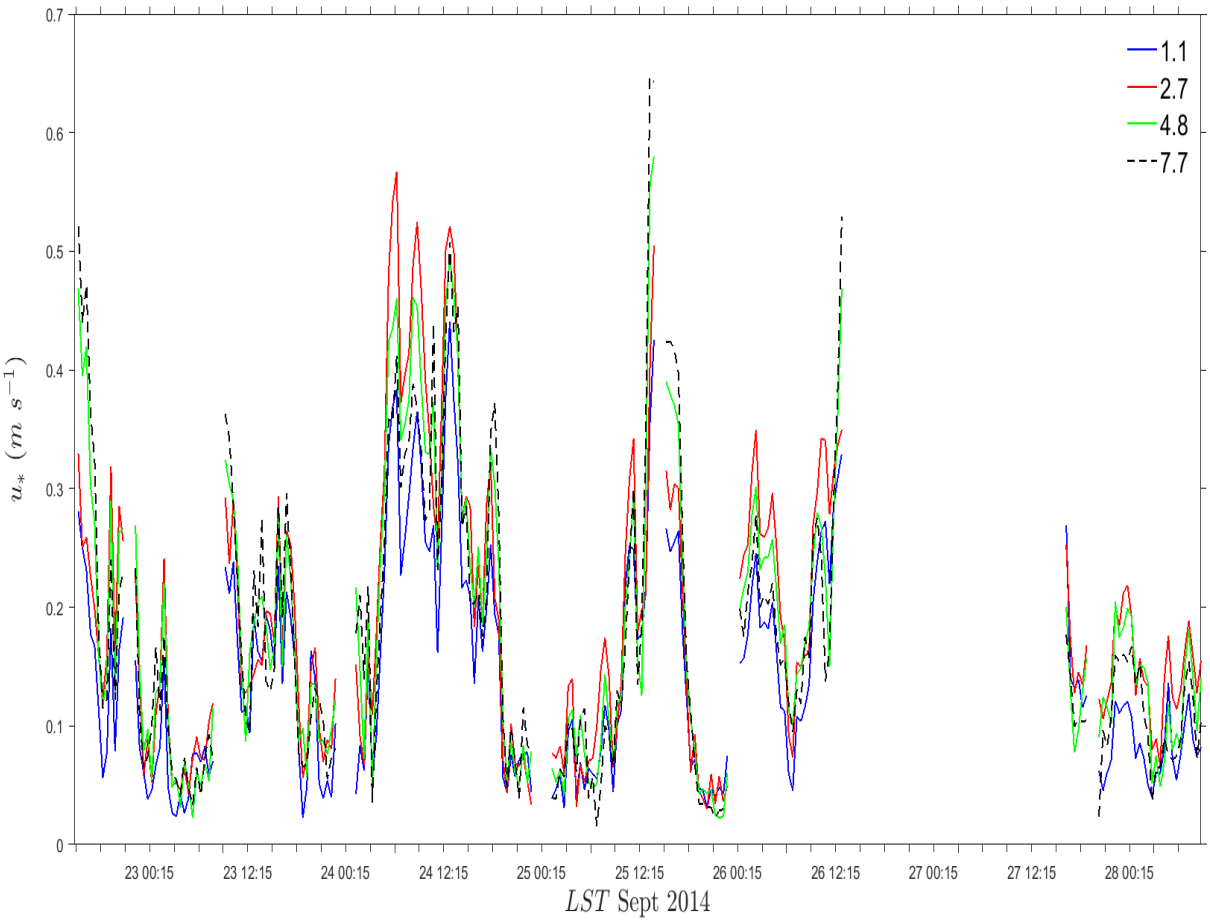

Figure 3.9. Diurnal variation of friction velocity (momentum flux) at four measurement heights 1.1m, 2.7m, 4.8m, and 7.7m at Echo, Oregon site from 22 September 2014 through 28 September 2014.

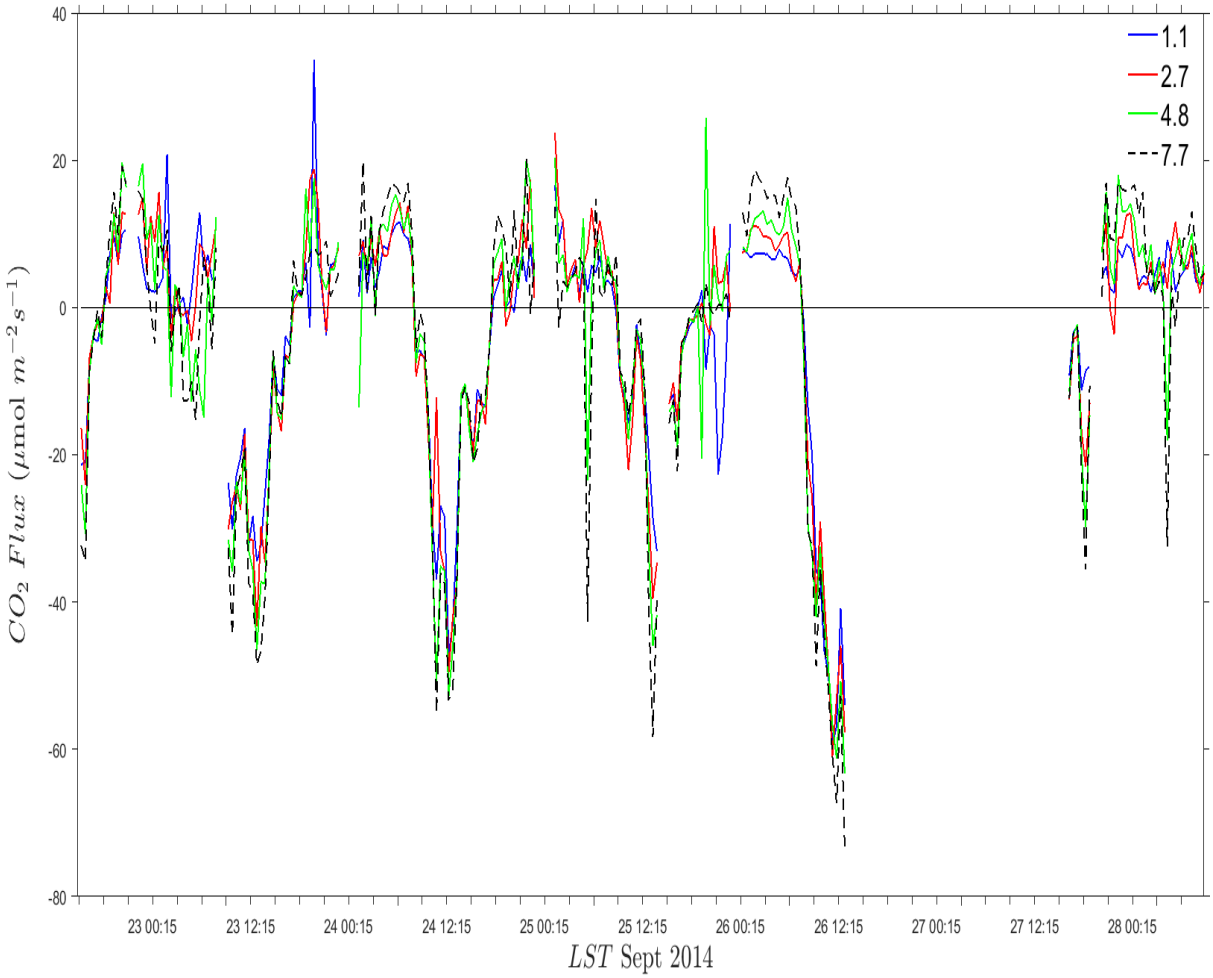

Figure 3.10. Diurnal variation of CO_2 flux at four measurement heights 1.1m, 2.7m, 4.8m, and 7.7m at Echo, Oregon from 22 September 2014 through 28 September 2014.

3.3 Impact of Mean-removal Time on Surface Fluxes

The surface flux data such as sensible heat flux, latent heat flux, momentum flux, and CO_2 flux were obtained from Reynolds decomposition, which is the process of removing turbulent motions from the mean (synoptic) motions. This was explained

in the methods section in the previous chapter. Three different time scales were used to remove the mean from the turbulent motions in this research to see how each surface flux is affected at different time scales. The time scales used were 5-minutes, 15-minutes, and 30-minutes, and flux calculations were based on a 30-minute averaging. However, the detrending time of 15-minutes was used in this research because we wanted to resolve for small eddies. Figures 3.11-3.14 show the plot of the surface fluxes at the different time scales as stated above. Some scientists have used different time scales to remove turbulent motions from the mean and observed that upward heat fluxes tend to increase with an increasing time scale during the daytime period, and small difference in fluxes was observed during stable periods [Vickers and Mahrt, 2003]. This hypothesis is also true in the plots presented with our data.

Figure 3.11 shows the diurnal pattern of sensible heat flux calculated using different time scales for mean-removal. The upward flux (positive flux) during the daytime period increased as the detrend time scale increased. But, there was little difference in fluxes observed during stable atmospheric conditions at nighttime. The latent heat flux presented in Figure 3.12 also showed a similar pattern to that of sensible heat flux. The exception is that the flux is higher at 15-minutes for a few days (22, 23, and 25 September 2014) in the data during the daytime compared to 5 and 30-minutes time scales.

Friction velocity, which is also known as the measure of momentum flux, was observed to increase with increasing mean-removal time scale during daytime as seen in Figure 3.13.

Vickers et al. [2003] did not include flux of CO_2 in their study to see whether or not it would behave similar to the turbulent fluxes of heat, moisture and momentum. This

research includes CO_2 flux, and the results presented in Figure 3.14 show that the downward flux of CO_2 increased in magnitude with an increased time scale for mean removal during the daytime.

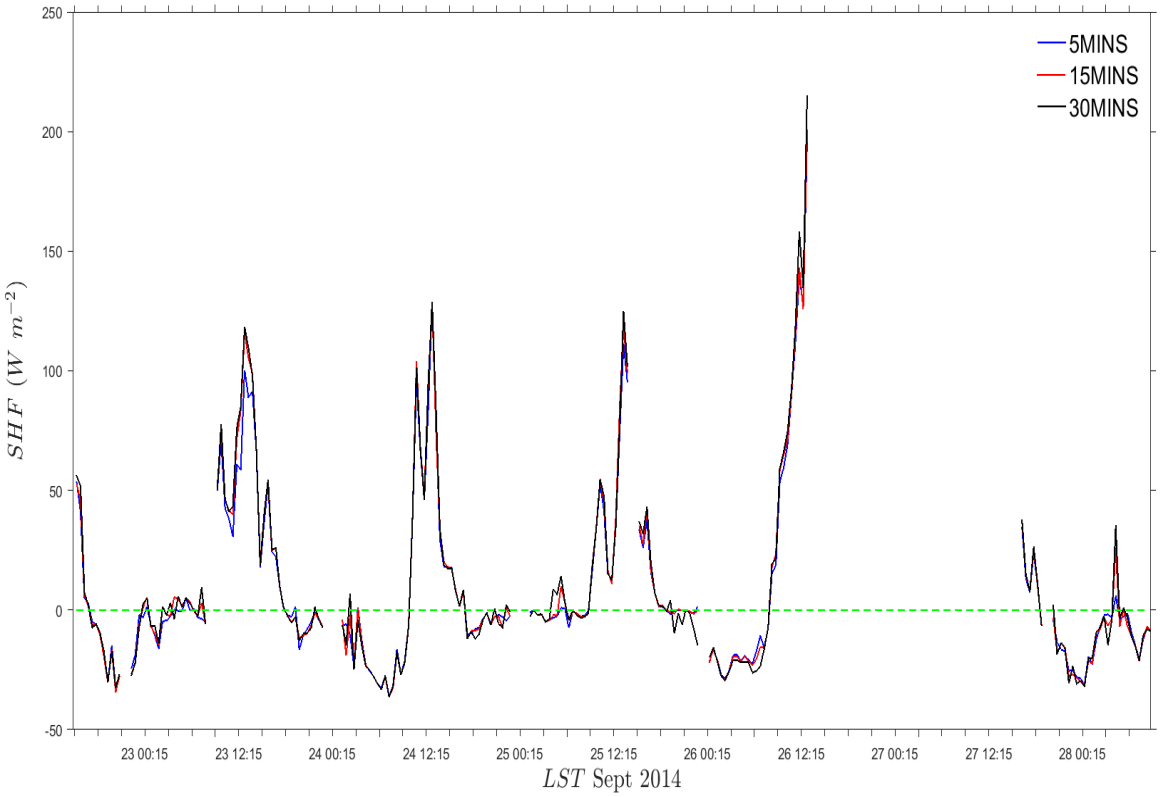

Figure 3.11. Diurnal variation of sensible heat flux at 3 different time scales for mean removal 5-minutes, 15-minutes, and 30-minutes at Echo, Oregon site from 22 September 2014 through 28 September 2014.

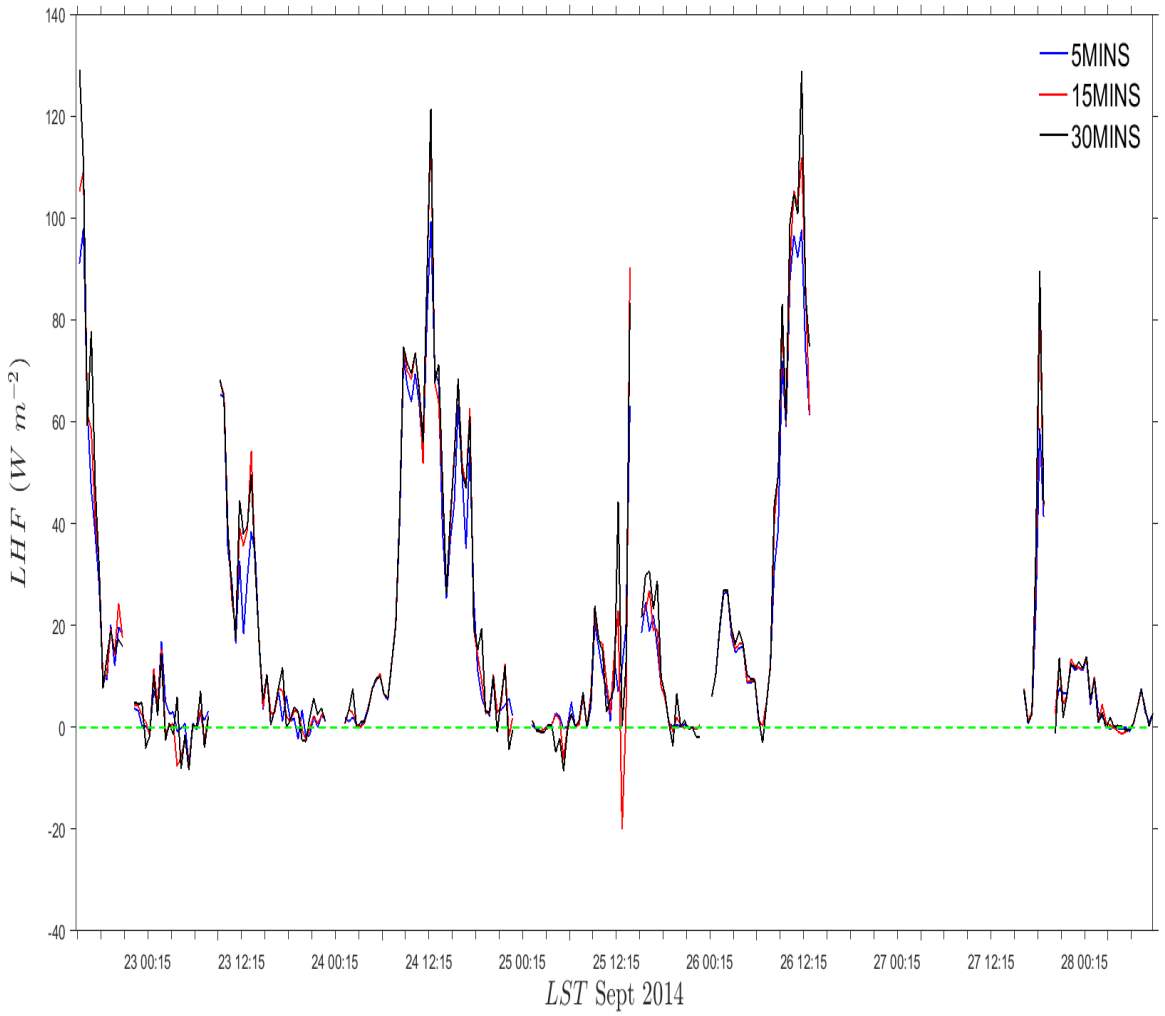

Figure 3.12. Diurnal variation of latent heat flux at 3 different time scales for mean removal 5-minutes, 15-minutes, and 30-minutes at Echo, Oregon from 22 September 2014 through 28 September 2014.

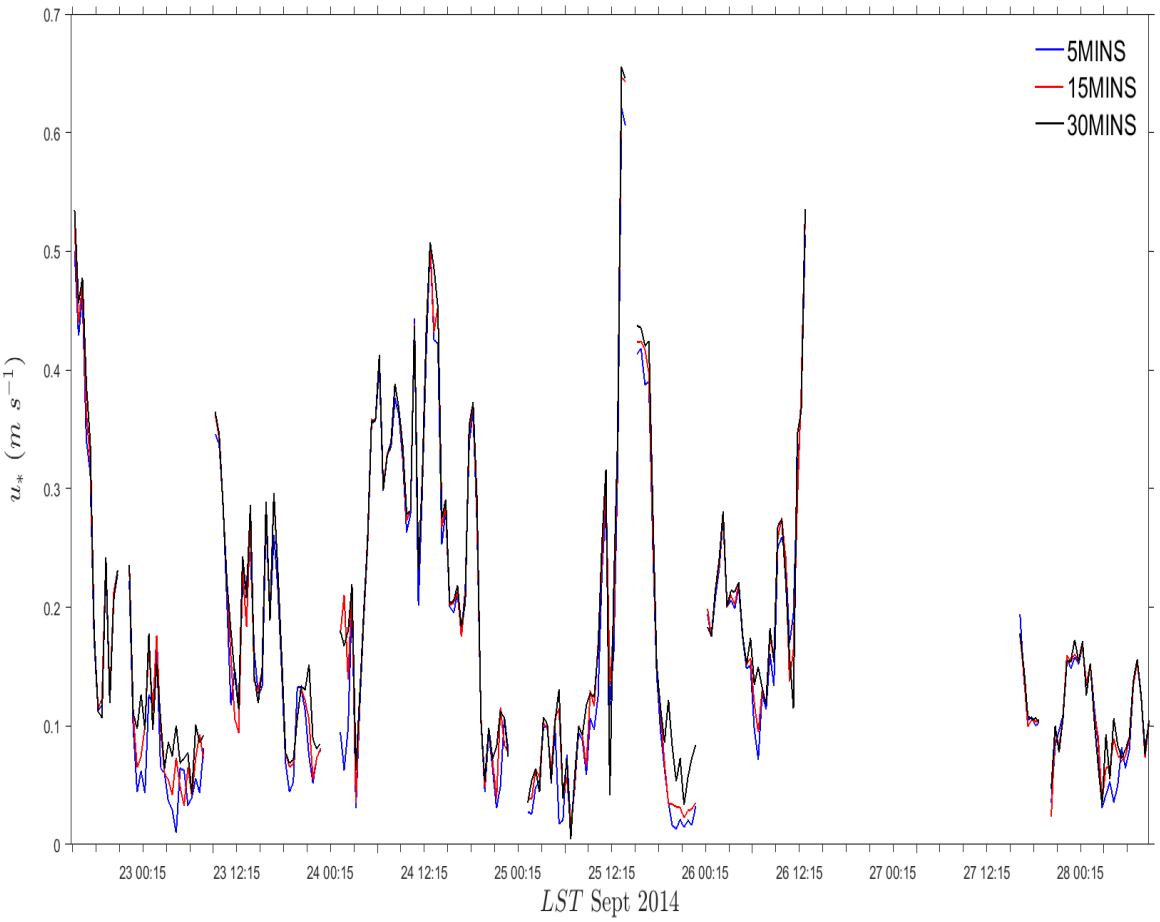

Figure 3.13. Diurnal variation of momentum flux (friction velocity) at 3 different time scales for mean removal 5-minutes, 15-minutes, and 30-minutes at Echo, Oregon from 22 September 2014 through 28 September 2014.

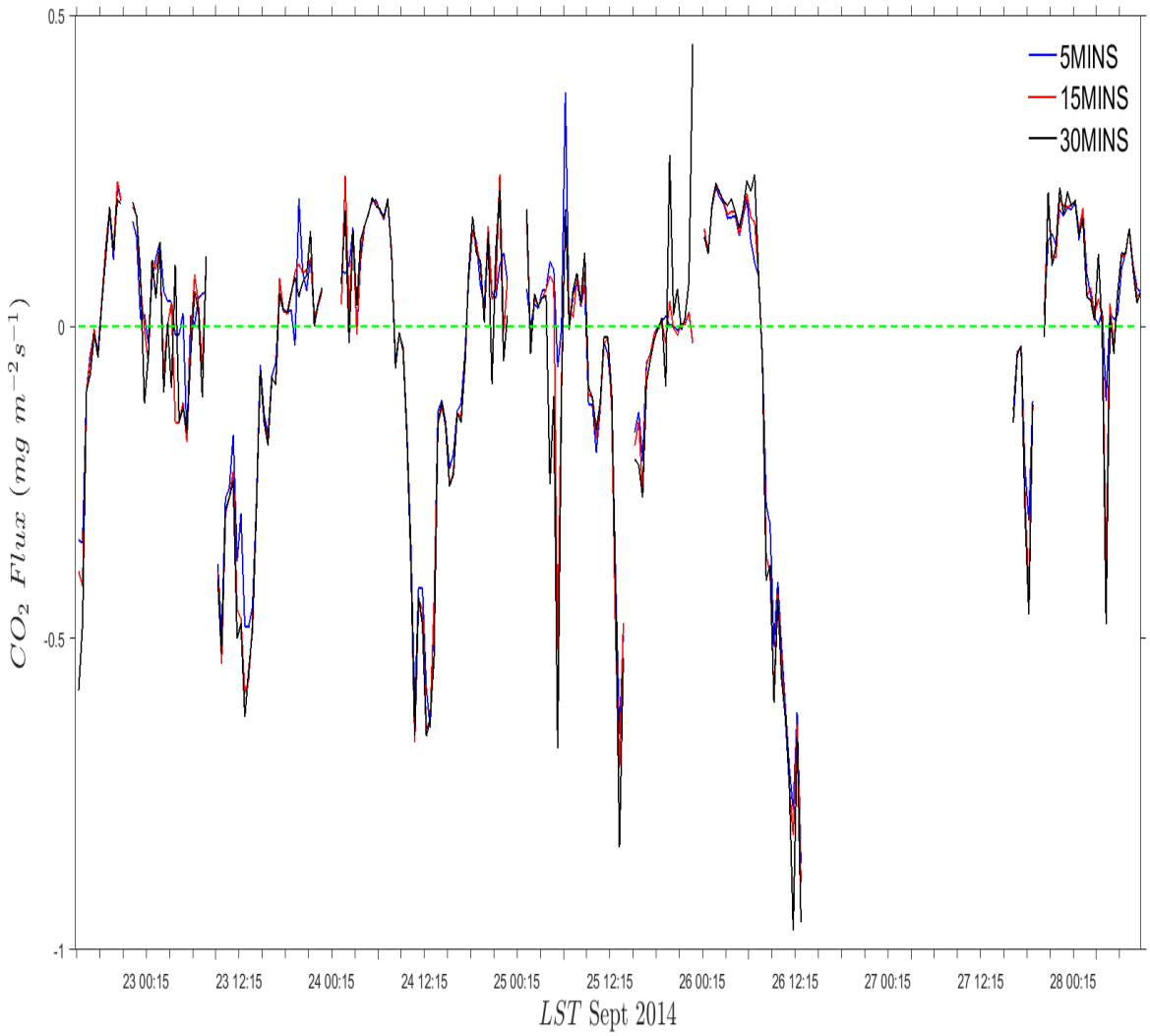

Figure 3.14. Diurnal variation of CO_2 flux at 3 different time scales for mean removal 5-minutes, 15-minutes, and 30-minutes at Echo, Oregon from 22 September 2014 through 28 September 2014.

3.4 Testing the Logarithmic Wind Profile Relationship in Rolling Terrain

The log law has been studied by several scientists within the atmospheric boundary layer and for flow within pipes based on the Reynolds number. Reynolds number is defined as the ratio between inertial and viscous forces in a flow, which

means a high Reynolds number is associated with high inertial forces. The log layer is formed during periods when the Reynolds number is high, which is the period when inertial forces dominate viscous forces. This has been studied in pipes, and wind tunnels. However, it is hard to maintain high Reynolds number in pipes and wind tunnel studies [George, 2007]. Our research uses the universal log law equation given in Equation (18) to determine the log wind profile in a planetary boundary layer, which would be difficult to achieve in this case because one of the assumptions required to achieve log law is a flat terrain but, our study site is rolling terrain (Figure 2.2).

Figure 3.15a presents the variation of wind speed logarithmically with height on a semi-log axis. The slope on the graph was derived as 1.6025, which determines the value of von Karman constant (k) as the inverse of the slope. The value of von Karman constant in this case is the inverse of 1.6025, which was obtained as ~0.61. The rougness length (z_o) was assumed to be 0.03 due to the surface properties of the study site [Stull, 1988]. However, this may not be accurate because there were sprinklers and wind turbines at the irrigated farmland near our study site, which are also referred to as roughness elements and the terrain is not flat.

Figure 3.15b shows the same plot as seen in Figure 3.14a. However, z_o was not assumed. It was obtained from the intercept of the plot as ~0.24 using Equation (18) and von Karman constant was determined to be ~0.33, which is the inverse of the slope. This is a bit closer to the accepted values of von Karman constant (0.35-0.40). The uncertainty in the slope and intercept was calculated in Figure 3.15b and the uncertainty in von Karman constant (k) was estimated as ± 0.09. The uncertainty in z_o

was estimated as ± 0.12.

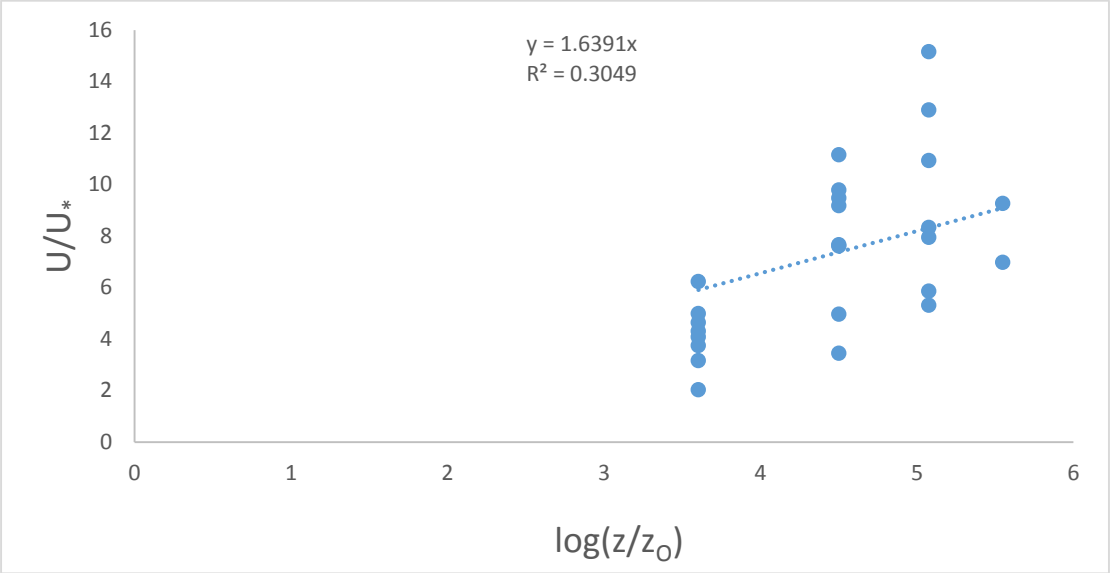

Figure 3.15a. Log wind profile in neutral atmospheric conditions assuming z_o is 0.03m.

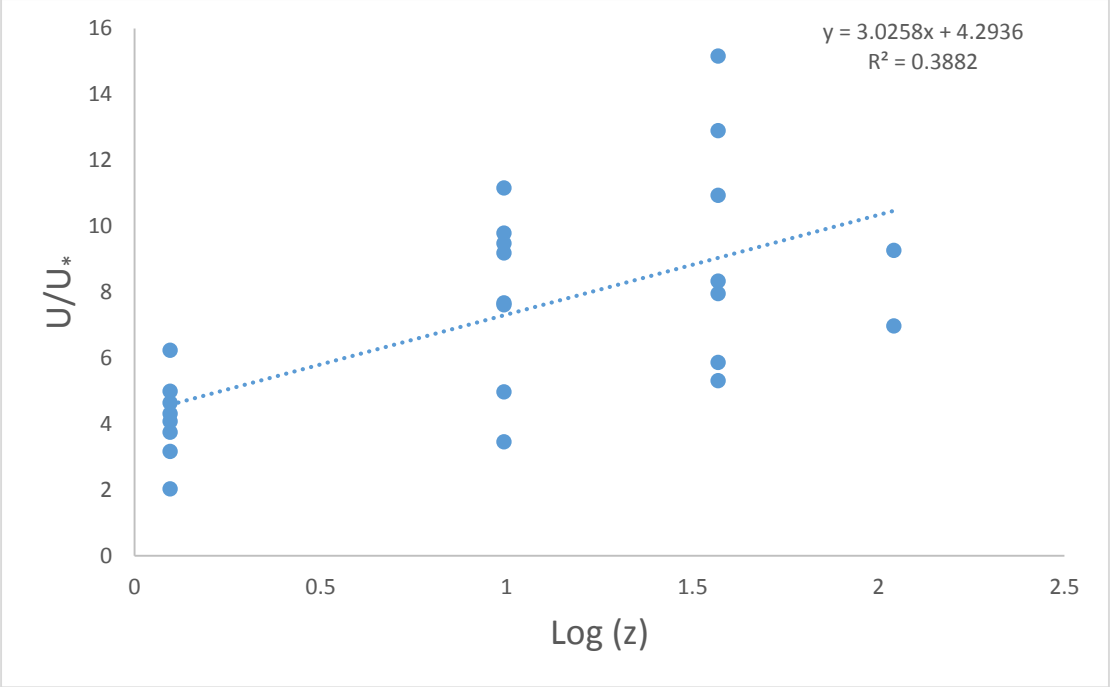

Figure 3.15b. Log wind profile in neutral atmospheric conditions with z_o obtained from the graph as 0.24m.

3.5 Relationship between Atmospheric Stability and Surface Fluxes

Atmospheric stability is used to describe the ability of the atmosphere to enhance or deter vertical motions. Scientists have discovered several methods of determining the stability of the atmosphere [Obukhov, 1971; Arya, 2001]. This research determined stability of the atmosphere using Monin-Obukov stability parameter given in Equations (13-16), and the temperature gradient. Figures 3.16-3.20 presents the correlation between temperature gradient and Monin-Obukov stability parameter as a measure of atmospheric stability and each of the surface fluxes.

Figure 3.16 displays the relationship between sensible heat flux and temperature gradient as a measure of atmospheric stability. The negative values of the

temperature gradient described unstable atmospheric conditions (enhanced vertical motion), while the positive values showed a period of stable atmospheric conditions. The positive temperature gradient also signifies a temperature inversion period (increase in temperature with height), the period when radiation cooling takes place at the surface due to more emission of long-wave radiation from Earth's surface at nighttime compared with absorption of sky long wave radiation. Sensible heat flux decreased as the temperature gradient increased. An upward flux of sensible heat was observed at a negative temperature gradient, which is reasonable during daytime, because convective turbulence at daytime is associated with a negative temperature gradient.

Latent heat flux showed a similar relationship with the temperature gradient to that of sensible heat flux as the flux decreased with the increased temperature gradient. A positive temperature gradient was observed at negative latent heat flux, while a negative temperature gradient was observed at a positive latent heat flux in Figure 3.17. This is reasonable because during periods of temperature inversion, the heat fluxes (latent and sensible heat) are usually pointing downward or near zero due to sinking air parcels at nighttime. The presence of clouds at nighttime would transmit long-wave radiation to the Earth's surface. But, in the absence of clouds, there is strong temperature inversion as the surface cools rapidly.

Figure 3.18 presents the relationship between the friction velocity (momentum flux) and temperature gradient, which showed a similar relationship as those of the heat and moisture fluxes. The friction velocity was higher during unstable atmospheric conditions (negative temperature gradient) and decreased as the

atmosphere transitions to stable conditions (positive temperature gradient). This is reasonable because friction velocity is a measure of atmospheric turbulence.

Figure 3.19 shows the relationship between CO_2 flux and temperature gradient. A positive temperature gradient (temperature inversion) occurred with a positive CO_2 flux and vice versa. This seems reasonable because positive CO_2 flux means the surface is emitting more CO_2 due to plants, soil respiration, and no sink for the CO_2 due to weak turbulent mixing, and shallow atmospheric boundary layer. The negative temperature gradient (an unstable atmospheric condition) was observed at the depletion of CO_2 concentration (a negative CO_2 flux) or uniformly mixed CO_2 concentration, and also driven by CO_2 uptake by plants.

Figure 3.20 presents the relationship between turbulent fluxes of moisture, heat, momentum, and CO_2. The fluxes of heat, moisture, and momentum were higher and concentrated at the early period of unstable atmospheric conditions (lower values of $z/L<0$) and became smaller during stable atmospheric conditions ($z/L>0$). The fluxes were also concentrated and high during neutral atmospheric conditions ($z/L=0$). During very unstable atmospheric conditions (lower values of $z/L<0$), the fluxes were more spread out and reduced. The downward flux (negative) of CO_2 was concentrated and stronger at the early period of unstable atmospheric conditions ($z/L<0$), and became more spread out and reduced during very unstable atmospheric periods (lower values of $z/L<0$). CO_2 flux became higher (positive) as the atmosphere transitions to stable conditions. The flux was concentrated and high during neutral atmospheric conditions and higher at the early period of stable atmospheric conditions. But, during very stable atmospheric periods, flux of CO_2 seems to flatten out to zero showing that it is no longer affected by the intensity of the stable periods.

Figure 3.21a presents the relationship between fetch and wind direction under different atmospheric stability conditions. Fetch can be described as the distance between the measuring sensor and the area contributing to the fluxes being measured. The fetch calculated in this study was larger during stable atmospheric conditions and the maximum fetch was obtained during south-west wind direction, which corresponds to the direction at which the sonic anemometer was aligned.

Figure 3.21b shows the average fetch estimated at different wind directions around the flux tower at the study site. The yellow mark at the center of the enclosed polygon represents the flux tower, while the inner polygon signifies the average fetch at different wind directions during unstable atmospheric conditions. The outer polygon represents the average fetch at different wind directions during stable atmospheric conditions. The fetch covers the irrigated farmland as seen in Figure 3.21b, which is reasonable in the results of our calculated surface fluxes.

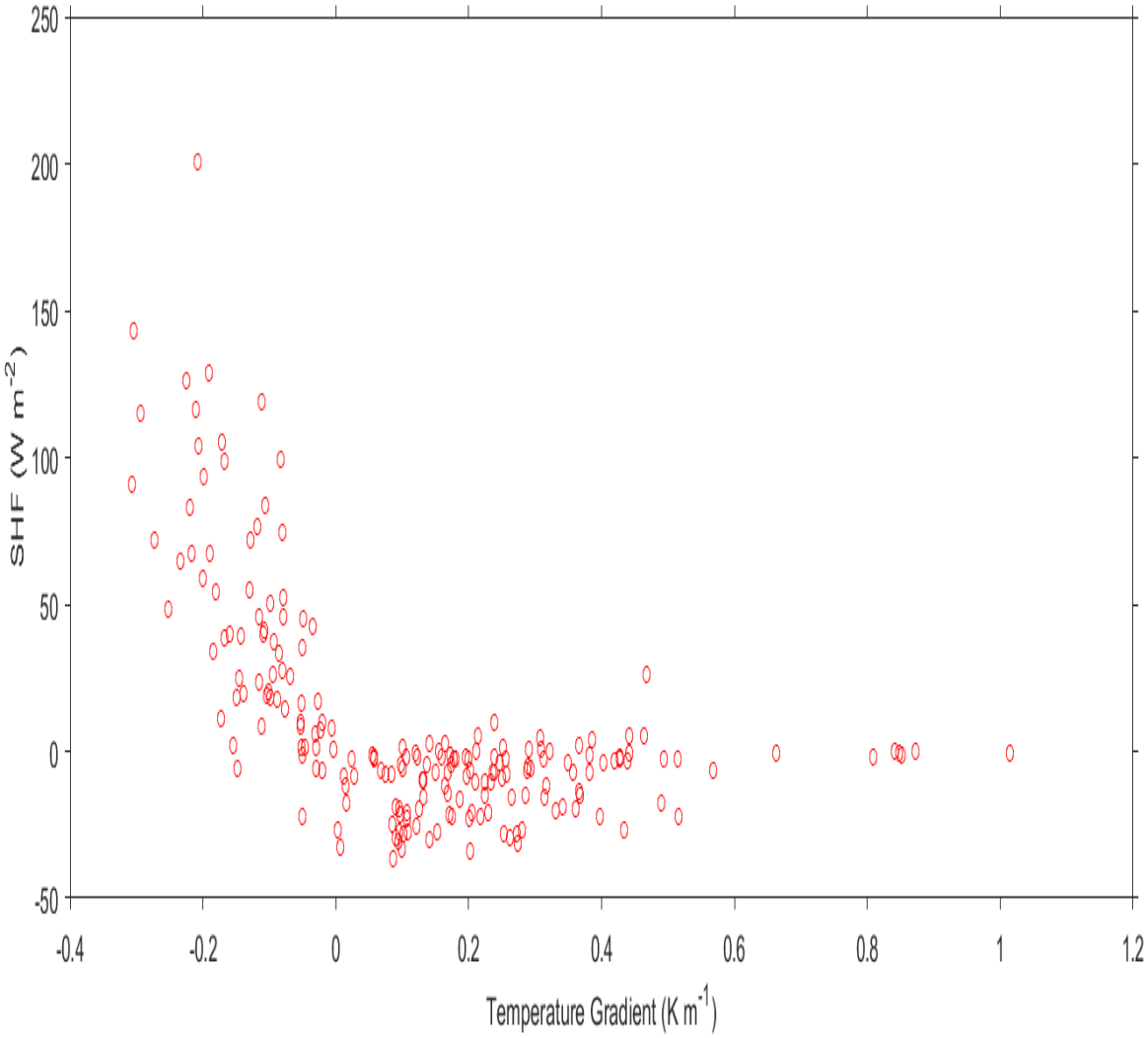

Figure 3.16. Relationship between sensible heat flux and temperature gradient at Echo, Oregon from 22 September 2014 through 28 September 2014.

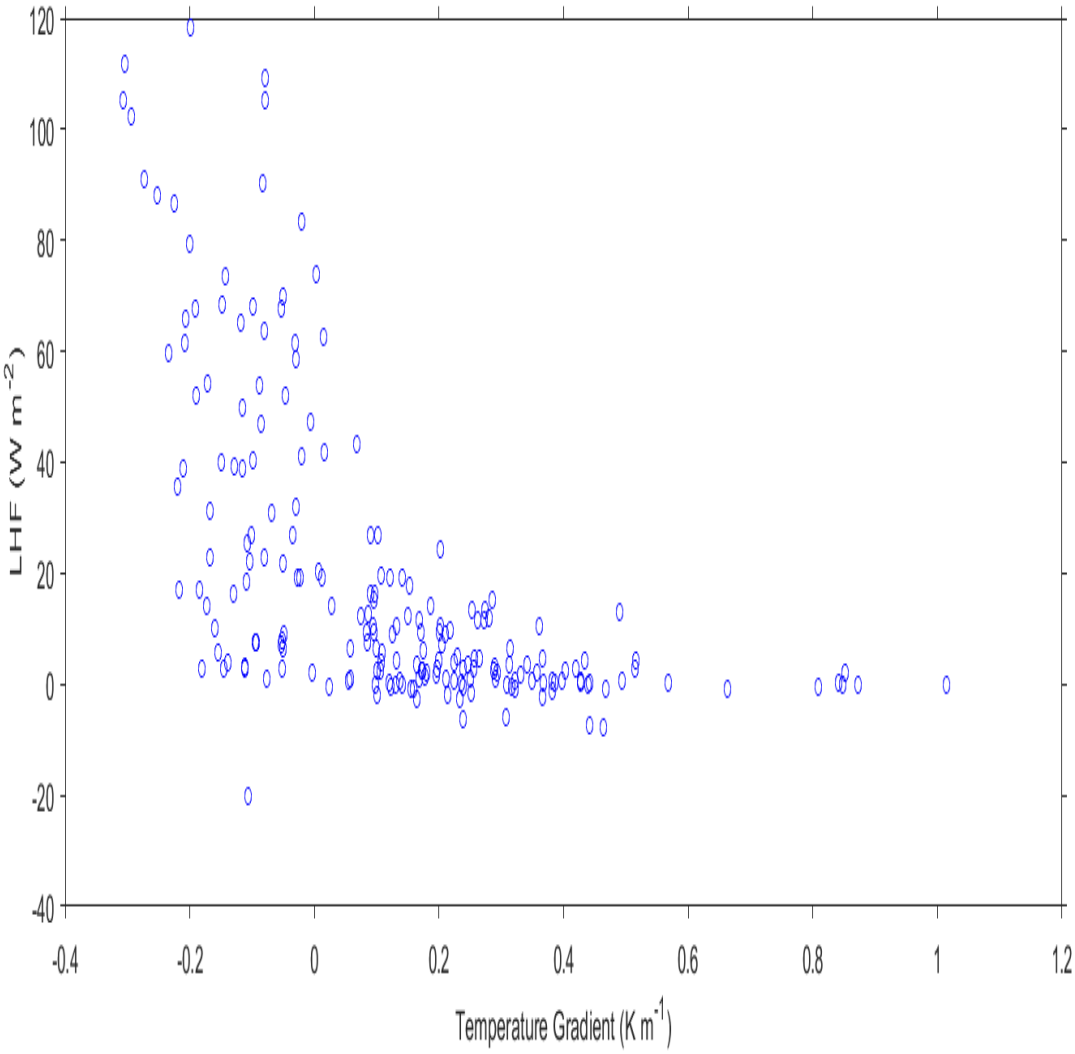

Figure 3.17. Relationship between latent heat flux and temperature gradient at Echo, Oregon from 22 September 2014 through 28 September 2014.

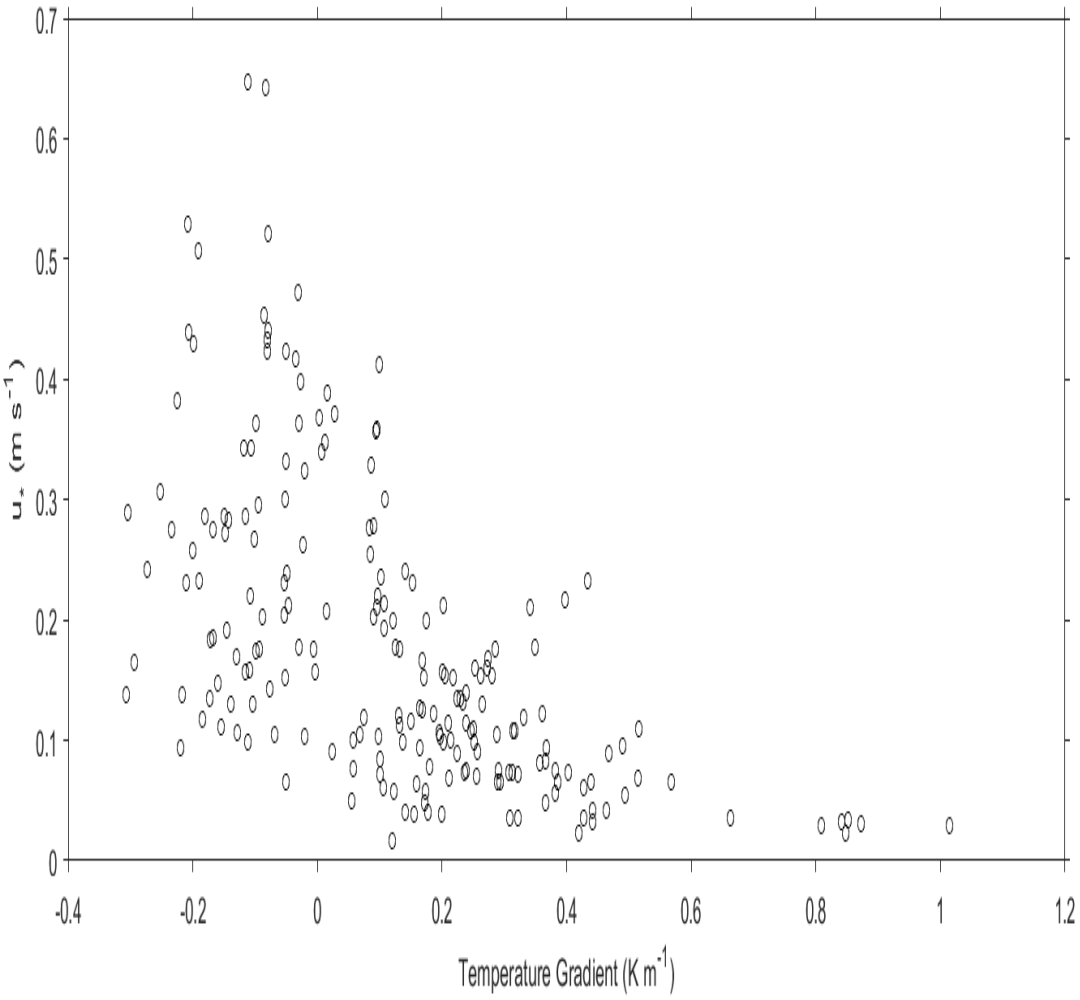

Figure 3.18. Relationship between friction velocity (momentum flux) and temperature gradient at Echo, Oregon from 22 September 2014 through 28 September 2014.

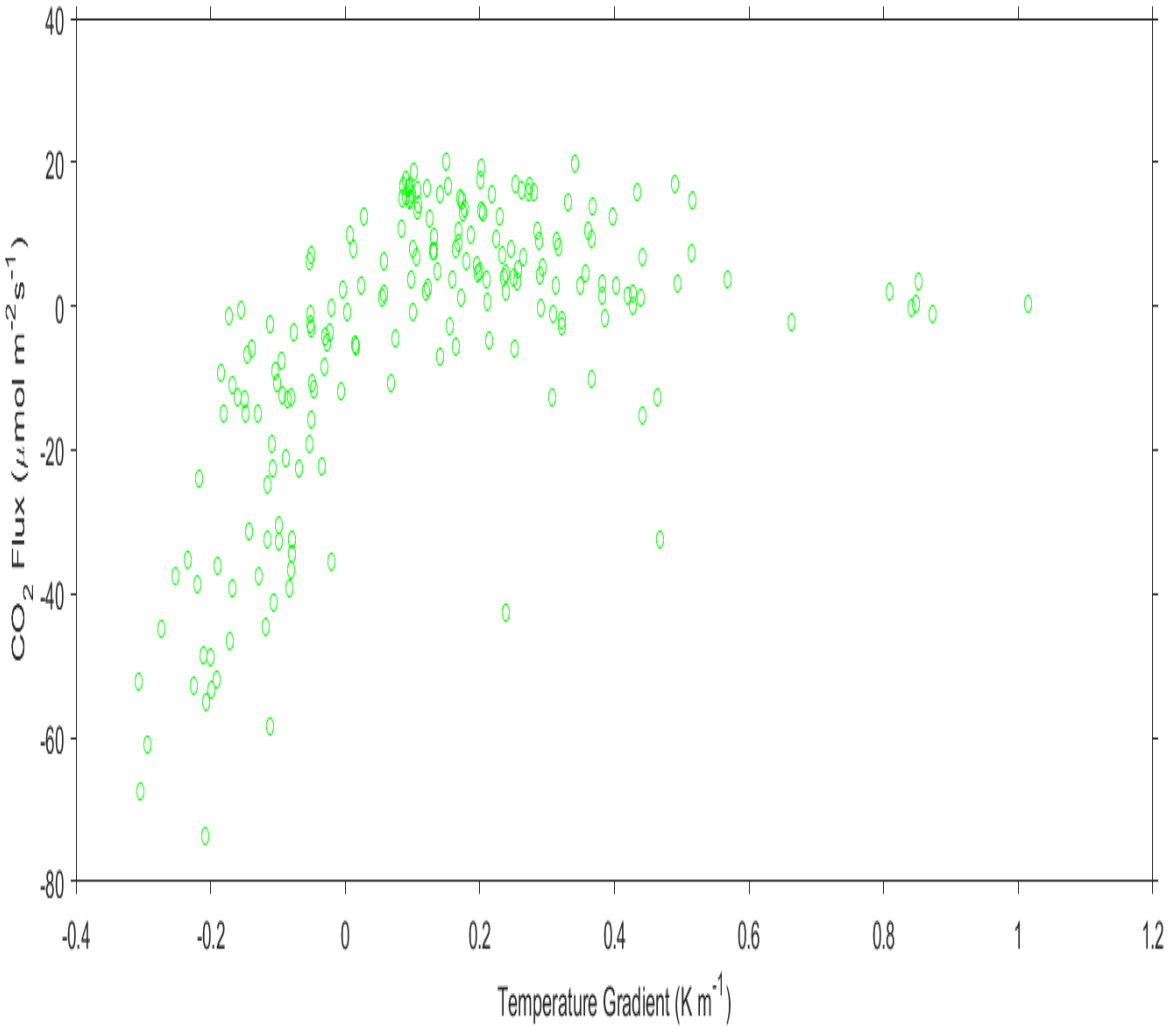

Figure 3.19. Relationship between CO_2 flux and temperature gradient at Echo, Oregon from 22 September 2014 through 28 September 2014.

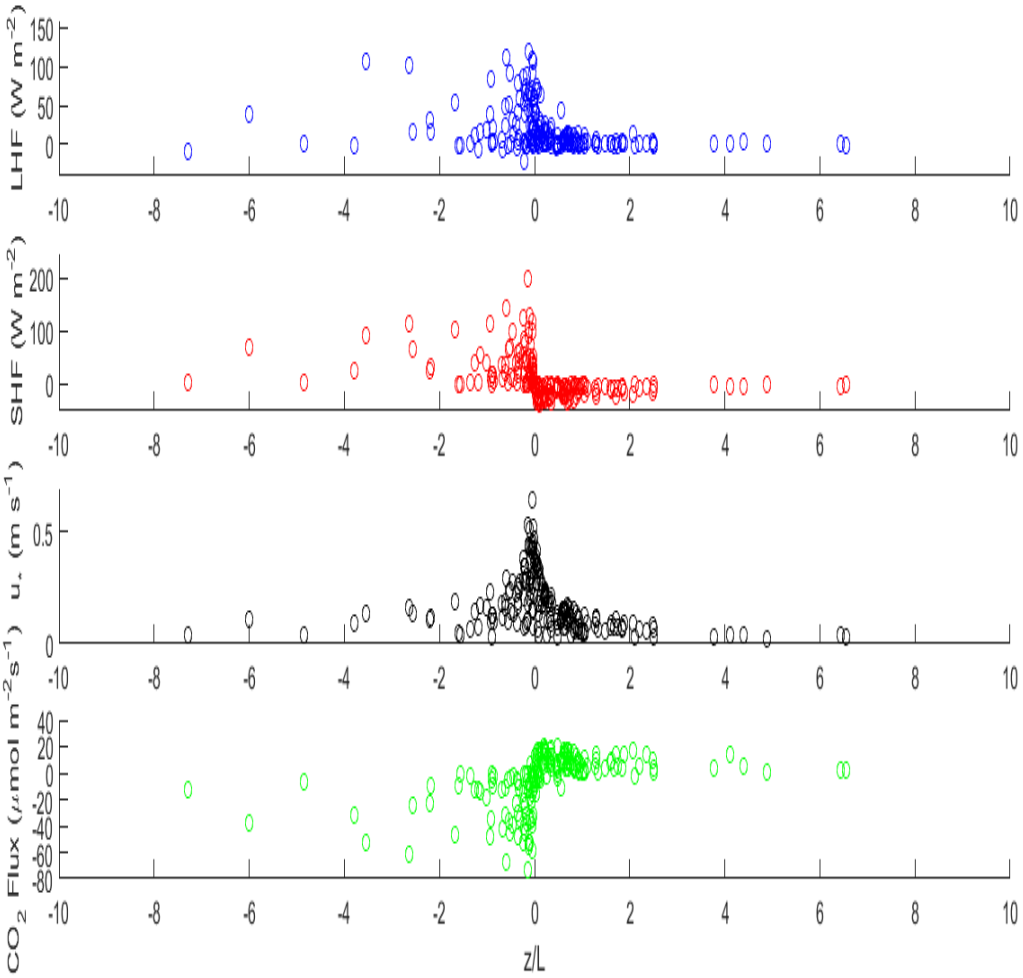

Figure 3.20. Relationship between turbulent fluxes of moisture, heat, momentum, CO_2 and Monin-Obukov stability parameter at Echo, Oregon from 22 September 2014 through 28 September 2014.

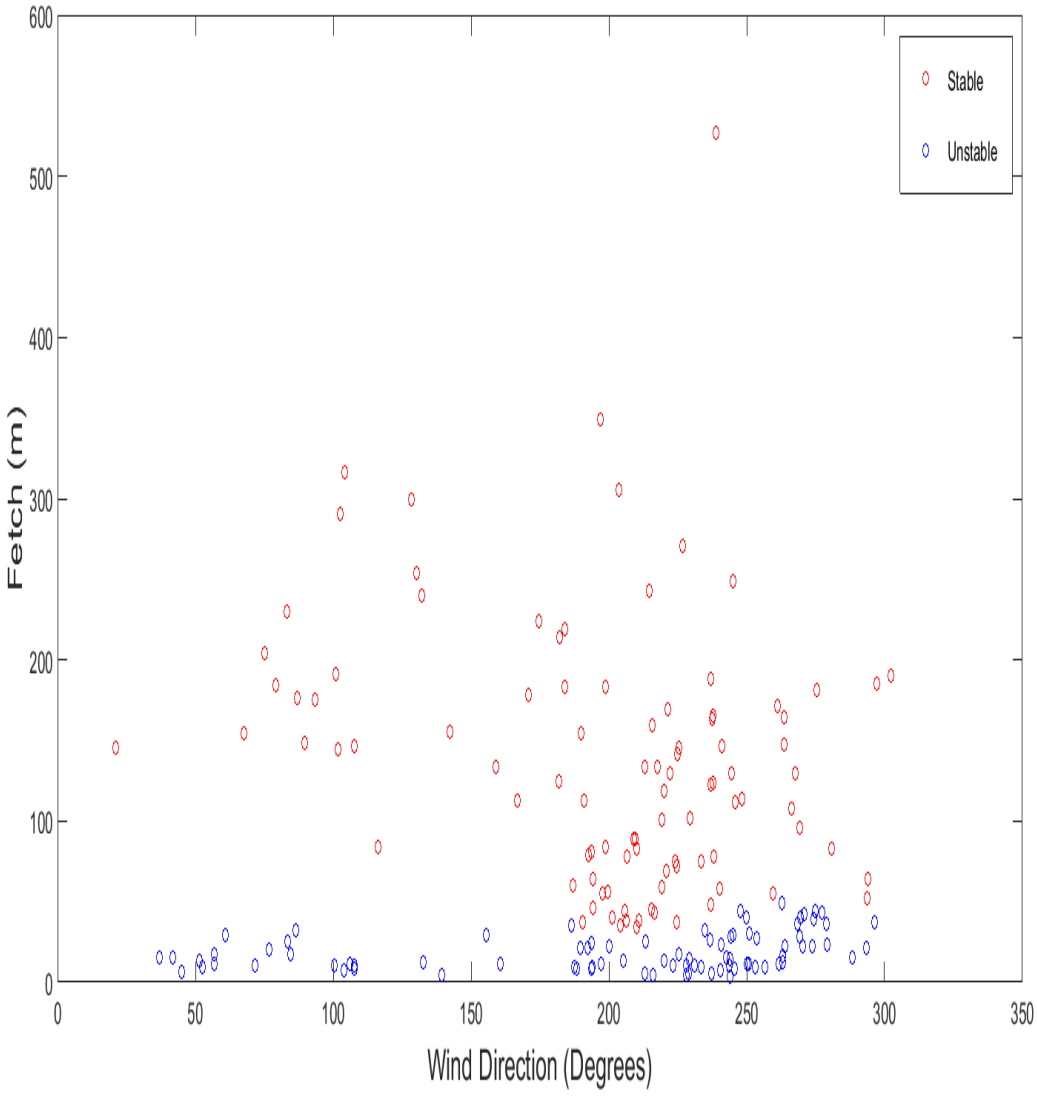

Figure 3.21a. Relationship between fetch and wind direction under different atmospheric stability conditions at Echo, Oregon from 22 September 2014 through 28 September 2014.

Figure 3.21b. Average fetch around the flux tower under unstable conditions (inner polygon) and stable conditions (outer polygon).

Chapter 4: Discussion

The results presented in this study indicate that topography has an influence on the estimated surface fluxes, especially the latent heat flux as moisture gradient was observed. This was a result of horizontal advection of moisture from the irrigated farmland near our study site. More so, the fetch estimated in this study was large during stable conditions, which is another point to buttress the point that horizontal advection influenced the estimated fluxes. This agrees with the findings of Lee and Hu [2002]. Topography could also prevent the momentum flux (friction velocity) from being constant with height. Terrain generates its own thermal circulations especially drainage flow at nighttime [Lee and Hu, 2002]. Temperature inversion and turbulence (strong winds) have a significant influence on turbulent exchange of heat, moisture, and CO_2. The role CO_2 and H_2O concentration play in the atmosphere is significant in altering the dynamics of the atmospheric boundary layer, which changes the surface energy balance. These are greenhouse gases that absorbs the heat (sensible and latent heat) emitted from the Earth's surface, radiating it back to the surface. This results in global warming.

The log law was investigated in our study to see if the log layer could be achieved at the study site, which is rolling terrain. The results can be compared to that of previous researchers [George, 2007]. Previous studies on CAP were conducted in a valley or basin during the winter season because insolation is typically low and convective mixing is inhibited within the boundary layer at daytime [Lareau et al., 2012; Holmes et al., 2015]. However, CAP was investigated in a basin at nighttime during a five day period in September 1999 in Utah [Clements et al., 2003], which is

in comparison with our study as temperature inversions was investigated in a small valley during one week in September 2014 in Echo, Oregon.

4.1 Investigating Log Law in Neutrally Stratified Boundary Layer

Log law in complex terrain is yet to be validated as most previous studies on log law focused on flat terrain, which is the ideal terrain required to achieve the log layer. Therefore, the law is expected to break down if applied to non-ideal terrain (complex terrain). This was observed in the result presented in our data for verifying the log law at the study site. Two log wind profiles were investigated (Figure 3.15a and b). The roughness length (z_o) was assumed to be 0.03m in Figure 3.15a because the surface consists of dry grass and patches of wet grass due to the irrigated farmland near the study site (Figure 2.2). The z_o value was adopted from Stull [1988] based on the surface properties classification. However, the von Karman constant (k) derived using the log wind profile (Figure 3.15a) is ~0.61 is not close to that of the accepted value, which is ~0.40. In Figure 3.15b, z_o was not assumed. It was determined from the log wind profile to be 0.24m and k was obtained as the inverse of the slope, which is ~0.33. This is close to the range of accepted values of k (0.35-0.40) probably because z_o was not assumed but determined using the log wind profile equation as seen in Equation (18) in Figure 3.15b.

The uncertainty in the slope and intercept was calculated and was used to estimate the uncertainty in the z_o and k. The obtained uncertainty in z_o is $\pm 0.09m$, while the uncertainty in k is ± 0.12. The second method used to determine k from logarithmic fitting of the wind speed (Figure 3.15b) is closer to accuracy. It is not a

surprise that the log law was not perfectly achieved in both methods employed in this research because the study site undermines one of the assumptions required for the log law to perform. More so, the surface property at the study site is a mixture of green, irrigated short grass, and dry patches of grass. This had much on the latent heat flux because moisture gradient was observed due to horizontal advection of moisture from the irrigated farmland near the study site. This means that the surface was not totally homogeneous, and this could be part of the reasons why the log law was not achieved in this research as the law also assumes surface homogeneity to work.

4.2 Temperature Inversion and Heat Fluxes

Temperature inversion in complex terrain can lead to CAP because cold air at the surface settles on the valley floor. The highest negative value of sensible heat flux (downward flux) observed on 24 September 2014 at nighttime is ~-42 Wm^{-2} compared to -60 Wm^{-2} reported by Clements et.al [2003] in a Utah basin. They stated that winds aloft broke into the basin to increase the downward flux of sensible heat (-60 Wm^{-2}) due to warm air advection. This fact is reflected by the observation in our study (Figure 3.9) as friction velocity increased with height at the same time (night time) the highest downward sensible heat flux was observed, and friction velocity as previously stated is a measure of mechanical turbulence (strong winds initiated by obstacles at the Earth's surface e.g., mountains, trees, grasses). The high downward fluxes of sensible heat reported by Holmes et.al [2015] were due to warm air advection over the cool surface, which caused an increase in wind speed during CAP and non-CAP periods. Another unique finding on sensible heat flux was on 25

September 2014 at night time when the downward flux was almost 0 unlike other days. This probably occurred due to the presence of clouds observed at the measurement site at that time, which means as the clouds emit more infrared radiation to the Earth's surface, the same amount of infrared radiation was been reflected from the surface since the surface is a strong absorber and emitter of infrared radiation, resulting in little sensible heat flux (near 0 W m^{-2}) at night time.

The latent heat flux was 0 Wm^{-2} on average during the nights, which means condensation might be taking place at the surface because it acts as a sink for H_2O despite the fact that there were light showers sometimes at night at the study site. Condensation usually occurs when air near the Earth's surface cools down below its saturation point at night time when the surface is colder than air aloft (temperature inversion period). This is observed in Figure 3.17 and 3.20 as the latent heat flux became 0 at a positive temperature gradient (temperature inversion) during stable atmospheric conditions (positive z/L).

4.3 Relationship between Temperature Inversion and CO_2 Concentration

Results showed that CO_2 concentration is higher at nighttime (Figure 3.6). The average night time CO_2 concentration is ~413 ppm compared to the average nighttime value of ~387 ppm reported by Reid and Steyn [1997] in a suburban region in Chicago during the summer in 1995. The average nighttime CO_2 concentration of 485 ppm was observed over a tropical forest [Culf et al., 1997]. This means that vegetation has a high impact on the atmospheric emission of CO_2 at nighttime due to plants, and soil respiration. The site used in our study is rural, and vegetation was the

primary source of CO_2 at the site. In addition, the exhaust from the generator used to power the sensors could have contributed to the sources of CO_2 concentration at our study site. The average nighttime CO_2 concentration observed by Grimmond et al.[2002] was 405 ppm, which was due to nocturnal or nighttime respiration, and shallow mixed layer heights.

During the strongest temperature inversion day (night time) on 26 September 2014 when CAP was felt in the small valley, maximum CO_2 concentration ~485 ppm was observed at the study site (Figure 3.6). This can be compared to the maximum nocturnal CO_2 concentration (441ppm) reported by Grimmond et al. [2002] in a suburban site that consisted of 36% buildings, 25% impervious, 7% trees and shrubs, and 32% grass in the summer (14 June-11 August) 1995. As previously stated, these researchers found that the maximum CO_2 observed was due to shallow boundary layer height at night time during stable atmospheric conditions, when the surface is colder than the air aloft. This agrees with the maximum CO_2 observed in our study on the strongest temperature inversion night.

4.4 Influence of Atmospheric Turbulence on Heat Fluxes

During the daytime, incoming solar radiation is absorbed by the Earth's surface, and as the surface heats the air directly above it, wind is generated and thermals of warm air rise (convection). This can also cause low level clouds called cumulus clouds to form. The winds generated are referred to as convective turbulence, which enhances the exchange of heat between the Earth's surface and atmosphere. In the presence of greenhouse gases (e.g., CO_2, H_2O), more longwave radiation is

radiated back to the surface and the surface [Grimmond and Oke, 1995] energy budget becomes imbalanced.

The typical daytime values of sensible heat flux are greater than 125 W m^{-2}. Maximum daytime sensible heat flux observed in Figure 3.7a is ~200 W m^{-2}, which was on 26 September 2014, the day after the strongest temperature inversion night. It was a clear sunny day at the measurement site, which means that the cold air on the valley floor the previous night was heated, eroding the CAP (transition from the previous night shallow boundary layer). There was a strong up-flow of warm air from the valley floor that resulted in high upward sensible heat flux, thus a thick boundary layer height. This maximum daytime value (200 W m^{-2}) can be compared to the maximum daytime value 292 W m^{-2}observed by some researchers in a hot and dry site in Tucson, Arizona [Grimmond and Oke, 1995] during the summer within 1990-1993. The researchers used four study sites (Tucson, Sacramento, Chicago, and Los Angeles) located in cities. The vegetation in each respective city was maintained by irrigation because rainfall was infrequent in all of the cities except Chicago. The maximum daytime values of sensible heat flux observed at each site (urban) in their study is greater than the maximum daytime value observed on our study site (rural). This may be due to the Urban Heat Island Effect, which depends on several factors e.g., limited moisture, urban structures (tall buildings), and atmospheric pollution [Bornstein, 1968]. More so, the building materials used in urban settings have high heat conductivity.

Latent heat flux was lower than sensible heat flux throughout our study period. This is reasonable because the study site is semi-arid. The climate of semi-arid regions generally has precipitation below potential evapotranspiration. Although it

rained sometimes at the study site, the farmland near the study site was well irrigated for adequate availability of moisture to plants. The maximum daytime latent heat flux (Figure 3.8) is ~118 W m^{-2} on 24 September 2014, which differs from the day maximum upward sensible heat flux was observed (26 September 2014). This agrees with the meteorological observations during that time, as it was windy (maximum wind speed ~5.8 m s^{-1} observed in Figure 3.3**)**, cloudy and stormy on 24 September 2014. Earlier that morning (~8am) the farmland nearby was irrigated, and this compounded with the rain impacted the maximum upward (daytime) latent heat flux. The cloudy sky might have attenuated the incoming solar radiation on this day, which could be the reason why maximum upward sensible heat flux was not observed until the clear sunny day of 26 September 2014. Despite that the sensible heat flux (~133 W m^{-2}) was not at maximum on 24 September 2014, it was still greater than the maximum upward latent heat flux at that time. Windy atmospheric conditions (turbulence) at the study site on the maximum upward latent heat flux day enhanced the evaporation process, which resulted in a maximum daytime (upward) latent heat flux.

In addition, observed strong winds (turbulence) might be responsible for the moisture gradient in Figure 3.5. It is interesting to observe an increase in moisture with height in this study, because generally moisture decreases with height because the surface is the source of moisture, so the farther away the atmosphere is from the surface, the more moisture is expected to decrease. However, this research shows an increase in moisture with height, and this can be associated with horizontal advection of moisture from the irrigated farmland near the study site. The fetch estimated shows that the irrigated farmland was within the area covered by the sensors (Figure 3.21b).

4.5 Influence of Atmospheric Turbulence on CO_2 Flux

Irrigated vegetation is a good source of carbon uptake. The irrigated farmland near the study site impacts not only the latent heat flux, but also the CO_2 flux (Figure 3.10). The negative flux of CO_2 during the daytime is a result of photosynthesis due to the presence of vegetation at the study site, which is in line with the findings from previous researchers [Grimmond et al., 2002; Ramamurthy and Pardyjak, 2011]. The positive upward fluxes of CO_2 at nighttime are due to plant and soil respiration, and small magnitudes due to decreased turbulence.

As stated in previous sections, atmospheric turbulence signifies periods of strong winds that are generated either convectively or mechanically. Atmospheric turbulence influences the exchange of CO_2 between the Earth's surface and the atmosphere because strong winds enhance photosynthesis processes as CO_2 is transported faster to plants, and mixing also takes place during this period, thus depleting the concentration of CO_2 within the atmospheric boundary layer (ABL). The most interesting finding presented in Figure 3.7a is on 26 September 2014 during daytime when the upward sensible heat flux was at maximum (~200 W m^{-2}), the downward flux of CO_2 was at maximum at the same time (~-73 μmol $m^{-2}s^{-1}$) in Figure 3.10. The maximum concentration of CO_2 (~485 ppm) the previous night decreased to ~375 ppm over the same period compared to the findings of Judd et al., [1993]. This means that there was a significant amount of the depletion of CO_2 concentration from the atmosphere, due to convective mixing and photosynthesis at

daytime. This can be compared to the maximum value reported by Ramamurthy et.al [2007], they observed a maximum CO_2 flux ~6 μmol $m^{-2}s^{-1}$ around 9am due to the peak traffic hour at one of their study sites. They used two study sites, suburban, and pre-urban with the presence of vegetation in only one of the sites. These researchers also found a relationship between sensible heat flux, and CO_2 flux. When sensible heat flux became positive, a huge spike was observed in the negative (downward) CO_2 flux, which was a result of a break up in accumulated CO_2 in the lower atmosphere during night time or early morning stable atmosphere, due to surface warming at daytime. However, the study site in our research is rural, and the primary source of CO_2 is vegetation.

Sensible heat flux determines the height of the boundary layer, which means as the upward sensible heat flux increases at daytime due to strong solar heating, the boundary layer height grows higher, and mixing is generated convectively. The strongest temperature inversion day (26 September 2014) at night time as discussed in the previous section had maximum CO_2 concentration, because there was no turbulence to mix out the emission of CO_2 respired from plants and soil to the plant canopy. Previous studies showed that the higher the flush out of CO_2 from plants to the atmosphere at early hours of the morning due to respiration, the higher the depletion of CO_2 from the atmosphere at daytime due to photosynthesis, and convective mixing [Culf et al., 1997].

4.6 Influence of Atmospheric Stability on Fetch

Fetch is defined as the distance between the measuring sensor and the boundary of the flux footprint. Flux footprint is an area upwind seen by sensors measuring vertical turbulent fluxes (e.g., heat, moisture, momentum, CO_2) such that the transport of the fluxes generated within this area are captured by the sensors. Fetch is less important on homogeneous surfaces because it is assumed that fluxes from all parts of the surface are equal [Schmid, 2002]. The fetch calculations in this study are based on the method developed by Hsieh et al. [2000] because their method describes the relationship between flux footprint, observation height, surface roughness, and atmospheric stability as given below:

$$x = \frac{D(z_u^P)(|L|^{1-P}}{2k^2}. \quad (19)$$

$$z_u = z_m[\left(\log\left(\frac{z_m}{z_o}\right)\right) - 1 + \left(\frac{z_o}{z_m}\right)]. \quad (20)$$

$D = 0.28, P = 0.59$ for unstable atmospheric conditions. (21)

$D = 2.44, P = 1.33$ for stable atmospheric conditions. (22)

$D = 0.97, P = 1$ for neutral atmospheric conditions. (23)

Where z_m is the measurement height (m), $z_o$is the roughness length (m), L is Monin-Obukov length (m), k is von Karman constant (0.4), D and P are similarity constants.

The higher the measuring sensor is from the ground, the more fetch it will have. So, in this study, the sensor at the upper level (7.7m) had more fetch than the sensor at 1.1m from the ground.

Figure 3.21a shows the relationship between wind direction, and fetch in different atmospheric stability conditions. The fetch is larger during stable atmospheric conditions, and smaller during unstable atmospheric conditions. reasonable because when the atmosphere is stable, there is a lateral flow, slow moving eddies, which means the measuring sensor captures a wider area contributing to the fluxes. However, the fetch was smaller during unstable atmospheric condition. This means that the measuring sensor could only capture the area closest to it because unstable atmospheric condition is a period of rapid motions, only fluxes within the area under the sensor or closest to it can be captured. This agrees with the findings of Horst [1999]. They found fetch to be smaller during unstable condition, and larger during stable atmospheric conditions using a different flux footprint model other than the one used in our research. The maximum fetch (~550 m) was found during stable atmospheric condition in the direction of the prevailing wind (south-west) in which the measuring sensor was aligned.

Chapter 5: Summary

Land-atmosphere exchange of heat, moisture, and CO_2 is crucial in boundary layer, air pollution, and climate studies. CO_2, and H_2O (moisture) are the greenhouse gases monitored in this research. These gases, when released into the atmosphere, trap heat emitted from the Earth's surface in form of longwave radiation, radiating it back to the surface, which causes a warmer temperature of the Earth. This phenomenon is known as greenhouse effect. This thesis presented one week of measurements (22 September 2014 – 28 September 2014) conducted in Echo, Oregon because it is semi-arid where high diurnal variation of measured meteorological variables is expected. In addition, the study site is rural, dominated mainly by vegetation, and generally only one vehicle passes a day, which means the major source of CO_2 emission at the site is vegetation and probably the exhaust from the generator used to power the sensors at the study site. Although, there were dry brown grasses around the study site where the tower was mounted, an irrigated farmland is located nearby, which is a good source of carbon exchange within the maximum fetch calculated in this research (~550m). The measurement site is in rolling terrain, and the tower was mounted in a small valley to isolate nighttime cold air pooling, and the sensors were placed at four heights (1.1m, 2.7m, 4.8m, and 7.7m) above the ground to calculate the gradients. The study aimed to demonstrate the influence of temperature inversion, and turbulence on surface fluxes of heat, moisture, and CO_2 using the eddy covariance technique to directly estimate the surface turbulent fluxes.

Meteorological data demonstrate strong diurnal variations in temperature, wind speed, wind direction, H_2O, and CO_2 concentrations. The strongest temperature

inversion was observed on 26 September 2014 (00:00-0100) as there were clear differences in temperature from the bottom sensor (1.1m) to the top sensor (7.7m) unlike during daytime when the temperature values at each level are almost the same due to convection as a result of surface heating from the sun. The temperature inversion was strongest on this day probably because it was a particularly clear night at the study site, suggesting that surface cooling was higher during this period because of the absence of clouds, and topography could also cause cold air to settle at the bottom of the valley intensifying the temperature inversion. This correlates to the maximum CO_2 concentration (~485 ppm) observed during this strong temperature inversion period. This suggests that as plants and soil respire emitting CO_2 into the atmosphere at nighttime, the concentration accumulated close to the ground due to a shallow boundary layer, and reduced turbulent mixing in the stable nocturnal boundary layer. However, during the daytime, sensible heat emitted from the Earth's surface resulting from surface heating by the sun caused the boundary layer height to grow, and convective turbulence enhanced photosynthesis; thus, CO_2 is depleted from the atmosphere. The average daytime CO_2 concentration (~388 ppm) was below the 2013 global average CO_2 (395 ppm), but the average nighttime CO_2 concentration (~407 ppm) was above the 2013 global average.

The wind direction during this research was on the average south-westerly, which correlates with the stormy, cloudy days that had rain at the measurement site because south-westerly winds are associated with moisture. In addition, the sensors were aligned at an angle 221^o, which corresponds to the south-west wind direction. There was a gradient in moisture and the latent heat flux increased with height from the surface, suggesting that the surface under the measuring sensor was not the source of

moisture; instead, it was probably advected from the irrigated farmland near the study site. Advection was also observed in the fluxes of CO_2 because the upward (positive) CO_2 flux increased with height during nighttime, and the downward (negative) flux of CO_2 increased with height during daytime on average, suggesting that the CO_2 emitted from irrigated vegetation nearby was transported to the study site through horizontal advection at nighttime, while the increased downward (negative) flux of CO_2 with height suggests high depletion rate of CO_2 from the atmosphere due to downward mixing of air at daytime.

It happened that the day (26 September 2014) immediately after the strongest temperature inversion was observed, the maximum sensible heat was recorded (~200 W m^{-2}). More so, the maximum upward sensible heat flux correlates with the maximum downward CO_2 flux (~$-74\ \mu mol\ m^{-2}s^{-1}$) during the same period at daytime (26 September 2014). This means that there is a relationship between sensible heat and CO_2 flux because sensible heat flux determines the growth of the boundary layer. The stronger the sensible heat flux, the higher the growth of the boundary layer, and the turbulent mixing layer. Moreover, turbulence enhances photosynthesis by transporting more CO_2 to plants rapidly (depletion of CO_2), and mixing CO_2 concentration in the atmosphere making it more uniformly spread.

The influence of temperature inversion, and turbulence on the turbulent fluxes of heat, moisture (latent heat), and CO_2 was presented in Figures 3.16-3.20. The heat fluxes (sensible, and latent heat flux) were higher during atmospheric turbulence/unstable atmospheric conditions (negative temperature gradient and negative z/L), and lower during temperature inversion/stable atmospheric conditions (positive temperature gradient and positive z/L), which suggests that heat, and

moisture are functions of atmospheric turbulence (strong winds). The fluxes of heat and moisture were also high during neutral atmospheric conditions (z/L = 0) due to mechanical turbulence. Atmospheric turbulence can be generated mechanically or convectively. The convective turbulence occurs as a result of strong surface heating by the sun at daytime giving rise to higher sensible heat flux with enhanced boundary layer growth. While, mechanical turbulence occurs when wind is generated behind surface roughness elements (e.g., trees and buildings). Strong winds drive evaporation yielding to higher magnitudes of latent heat fluxes. The downward flux of CO_2 is also higher in magnitude during strong winds due to turbulent mixing, and the photosynthetic activities during the daytime. While a temperature inversion reduces the fluxes of heat and moisture, the upward fluxes of CO_2 were increased due to plants, soil respiration with shallow boundary layer, weak turbulent mixing, and stable nocturnal boundary layer.

The limitation observed in this study is that the eddy covariance method used to estimate the turbulent fluxes assumes horizontally uniform surface, which means advective effects are not expected. However, advection of moisture from the irrigated farmland near the study site was observed as the latent heat flux increased with height throughout the measurement period. More so, there was advection of CO_2 from the same farmland as there was gradient in the CO_2 flux on average. The study site also is rolling terrain (Figures 2.1-2.2), and the method is ideal on relatively flat terrain. In addition, MOST was used to calculate the Monin-Obukov length, and Obukov stability parameter in this research. However, the theory is ideal for relatively flat terrain meaning that it may perform well if used in non-ideal terrain such as, rolling or complex terrain. This is one of the reasons why boundary layer models such as,

Weather Research Forecast model (WRF) fail especially during stable atmospheric conditions because the model uses MOST.

In addition, this study is crucial to air pollution studies because CO_2 has been considered as an air pollutant, and it is important to monitor CO_2 exchange between the Earth's surface and the atmosphere. CO_2 is a greenhouse gas that alters boundary layer dynamics through the process of global warming if released into the atmosphere. Previous studies have monitored CO_2 exchange in both urban and rural regions with the findings that CO_2 emissions are higher in urban sites than rural sites due to more contribution from anthropogenic sources (e.g., vehicles, and industries) and in the absence of vegetation in cities (urban), there is no sink for it. Despite that the study site used in this research is rural where vegetation was the major source of CO_2 and probably the exhaust from the generator used at the study site to power measuring instruments, maximum concentration (~485 ppm) was observed on the strongest temperature inversion day at nighttime, which is higher than the 2013 global average CO_2.

The log law (for neutrally stratified conditions) was not valid for rolling terrain in our study as the value of von Karman constant (~0.61) derived from the log wind profile using the method described in Figure 3.15a is not close to the accepted von Karman (k) constant value of about 0.40. However, the approach taken to obtain k (~0.33) in Figure 3.15b is very close to the accepted range of values (0.35-0.40). Although, we didn't determine k to be 0.40. The uncertainty in the obtained k in Figure 3.15b is ± 0.09, which means within the uncertainty, k was ~0.42.The correlation coefficient (R^2) obtained in the log wind profile is low and it could be that the uncertainty in the slope and intercept are affected by rolling terrain. The results

from this study can be compared with that of WRF model output for future studies with the aim of improving boundary layer models. More boundary layer studies are needed in rolling terrain to improve the methods currently available for estimating turbulent surface fluxes because the assumptions required to apply the eddy covariance method, for example, are not appropriate for complex terrain.

Appendix A

CODES USED FOR DATA PROCESSING

The Matlab codes, with description used to postprocess the IRGASON and sonic anemometer CSAT3 data are given in this section.

A.1 Postprocessing Data Taken in Echo, Oregon 2014

The codes are used to extract IRGASON and sonic anemometer CSAT3 data into separate binary files to be used in further calculations. The codes are to be run in the order listed except stated otherwise.

ExtractSonicBinary.m— This Prompts user for *.TOB file and then breaks up the Sonic Data into separate binary data files.

SonicDiagnosticSingle.m— This is a function to get rid of NaNs in time series sonic data.TimeGapFix.m— This is a function to interpolate data for missing time gap data in time series sonic data.

A.2 Calculations

After all data have been extracted into separate binary files in Matlab codes, then calculations can be done using the codes below. The codes are also used for generating figures.

PlanarFit.m— This is used for sonic tilt correction.

Lin_detrend_avg.m—Linearly detrends the time series data to obtain turbulent

fluctuations for ux, uy, uz, and Ts.

LinearDetrendIRGA.m— Linearly detrends the time series data to obtain turbulent fluctuations for CO_2 and H_2O.

CalcSonicTurbData.m— This calculates all the surface fluxes based on the averaging times.

CO2Convert.m— This converts the CO2 concentration from mg m^{-3} to ppm.

FluxFootprint_zo.m— This is used to calculate the fetch of the fluxes measured.

A.3 Uncertainty in Log wind profile obtained roughness length (zo) and von Karman Constant (k)

$\frac{U}{u_*} = \frac{1}{k} ln(\frac{z}{z_o})$. log wind profile equation (A1)

On y-axis is $\frac{U}{u_*}$ and x-axis is lnz.

Re-arranging the log wind profile equation yields:

$$\frac{U}{u_*} = \frac{1}{k} lnz - \frac{1}{k} lnz_o. \quad (A2)$$

Assume the slope to be m = $\frac{1}{k}$, and the intercept is assumed to be B= $-\frac{1}{k} lnz_o$.

(A3)

Then, re-arranging Equation (A3) gives;

$$lnz_o = -\frac{B}{m} \quad . \quad (A4)$$

$$z_o = \exp(-\frac{B}{m}) \quad . \quad (A5)$$

Then, uncertainty in z_o is calculated as:

$$\Delta z_o = \sqrt{(\frac{\partial z_o}{\partial B}\Delta B)^2 + (\frac{\partial z_o}{\partial m}\Delta m)^2} \quad . \quad (A6)$$

$$\frac{\partial e^{-\frac{B}{m}}}{\partial B} = \sqrt{(-\frac{1}{m} e^{-\frac{B}{m}}\Delta B)^2 + (-\frac{B}{m^2} e^{-\frac{B}{m}}\Delta m)^2} \quad . \quad (A7)$$

The uncertainty in k is calculated as:

$$\Delta k = \frac{\partial k}{\partial m}\Delta m = k\frac{\Delta m}{m} = \frac{k}{m} \quad . \quad (A8)$$

References

Arya, S. P. (2001), *Introduction to Micrometeorology*, Academic Press.

Baker, K. R., H. Simon, and J. T. Kelly (2011), Challenges to Modeling "Cold Pool" Meteorology Associated with High Pollution Episodes, *Environ. Sci. Technol.*, *45*(17), 7118–7119, doi:10.1021/es202705v.

Baldocchi, D., J. Finnigan, K. Wilson, K. T. P. U, and E. Falge (2000), On Measuring Net Ecosystem Carbon Exchange Over Tall Vegetation on Complex Terrain, *Bound.-Layer Meteorol.*, *96*(1–2), 257–291, doi:10.1023/A:1002497616547.

Baldocchi, D. et al. (2001), FLUXNET: A New Tool to Study the Temporal and Spatial Variability of Ecosystem–Scale Carbon Dioxide, Water Vapor, and Energy Flux Densities, *Bull. Am. Meteorol. Soc.*, *82*(11), 2415–2434, doi:10.1175/1520-0477(2001)082<2415:FANTTS>2.3.CO;2.

Baldocchi, D. D. (2003), Assessing the eddy covariance technique for evaluating carbon dioxide exchange rates of ecosystems: past, present and future, *Glob. Change Biol.*, *9*(4), 479–492, doi:10.1046/j.1365-2486.2003.00629.x.

Banta, R. M., L. D. Olivier, W. D. Neff, D. H. Levinson, and D. Ruffieux (1995), Influence of canyon-induced flows on flow and dispersion over adjacent plains, *Theor. Appl. Climatol.*, *52*(1–2), 27–42, doi:10.1007/BF00865505.

Barr, S., and M. M. Orgill (1989), Influence of External Meteorology on Nocturnal Valley Drainage Winds, *J. Appl. Meteorol.*, *28*(6), 497–517, doi:10.1175/1520-0450(1989)028<0497:IOEMON>2.0.CO;2.

Bornstein, R. D. (1968), Observations of the Urban Heat Island Effect in New York City, *J. Appl. Meteorol.*, *7*(4), 575–582, doi:10.1175/1520-0450(1968)007<0575:OOTUHI>2.0.CO;2.

Brutsaert, W. (1998), Land-surface water vapor and sensible heat flux: Spatial variability, homogeneity, and measurement scales, *Water Resour. Res.*, *34*(10), 2433–2442, doi:10.1029/98WR01340.

Businger, J. A., J. C. Wyngaard, Y. Izumi, and E. F. Bradley (1971), Flux-Profile Relationships in the Atmospheric Surface Layer, *J. Atmospheric Sci.*, *28*(2), 181–189, doi:10.1175/1520-0469(1971)028<0181:FPRITA>2.0.CO;2.

Clements, C. B., C. D. Whiteman, and J. D. Horel (2003), Cold-Air-Pool Structure and Evolution in a Mountain Basin: Peter Sinks, Utah, *J. Appl. Meteorol.*, *42*(6), 752–768, doi:10.1175/1520-0450(2003)042<0752:CSAEIA>2.0.CO;2.

Contini, D., A. Donateo, C. Elefante, and F. M. Grasso (2012), Analysis of particles and carbon dioxide concentrations and fluxes in an urban area: Correlation with traffic rate and local micrometeorology, *Atmos. Environ.*, *46*, 25–35, doi:10.1016/j.atmosenv.2011.10.039.

Culf, A. D., G. Fisch, Y. Malhi, and C. A. Nobre (1997), The influence of the atmospheric boundary layer on carbon dioxide concentrations over a tropical forest, *Agric. For. Meteorol.*, *85*(3–4), 149–158, doi:10.1016/S0168-1923(96)02412-4.

Drake, B. G., and M. A. Gonzàlez-Meler, and S. P. Long (1997), MORE EFFICIENT PLANTS: A Consequence of Rising Atmospheric CO2?, *Annu. Rev. Plant Physiol. Plant Mol. Biol.*, *48*(1), 609–639, doi:10.1146/annurev.arplant.48.1.609.

Dyer, A. J., and B. B. Hicks (1970), Flux-gradient relationships in the constant flux layer, *Q. J. R. Meteorol. Soc.*, *96*(410), 715–721, doi:10.1002/qj.49709641012.

Foken, T. (2006), 50 Years of the Monin–Obukhov Similarity Theory, *Bound.-Layer Meteorol.*, *119*(3), 431–447, doi:10.1007/s10546-006-9048-6.

Foken, T. (2008), *Micrometeorology*, Springer Science & Business Media.

Froelich, N. J., and H. P. Schmid (2006), Flow divergence and density flows above and below a deciduous forest: Part II. Below-canopy thermotopographic flows, *Agric. For. Meteorol.*, *138*(1–4), 29–43, doi:10.1016/j.agrformet.2006.03.013.

Froelich, N. J., H. P. Schmid, C. S. B. Grimmond, H.-B. Su, and A. J. Oliphant (2005), Flow divergence and density flows above and below a deciduous forest: Part I. Non-zero mean vertical wind above canopy, *Agric. For. Meteorol.*, *133*(1–4), 140–152, doi:10.1016/j.agrformet.2005.09.005.

Fuehrer, P. L., and C. A. Friehe (2002), Flux Corrections Revisited, *Bound.-Layer Meteorol.*, *102*(3), 415–458, doi:10.1023/A:1013826900579.

Garratt, J. R., and others (1992), The atmospheric boundary layer, Cambridge atmospheric and space science series, *Camb. Univ. Press Camb.*, *416*, 444.

Geiss, A., and L. Mahrt (2015), Decomposition of Spatial Structure of Nocturnal Flow over Gentle Terrain, *Bound.-Layer Meteorol.*, *156*(3), 337–347, doi:10.1007/s10546-015-0043-7.

Geissbühler, P., R. Siegwolf, and W. Eugster (2000), Eddy Covariance Measurements On Mountain Slopes: The Advantage Of Surface-Normal Sensor Orientation Over A Vertical Set-Up, *Bound.-Layer Meteorol.*, *96*(3), 371–392, doi:10.1023/A:1002660521017.

George, W. K. (2007), Is there a universal log law for turbulent wall-bounded flows?, *Philos. Trans. R. Soc. Lond. Math. Phys. Eng. Sci.*, *365*(1852), 789–806, doi:10.1098/rsta.2006.1941.

Goulden, M. L., J. W. Munger, S.-M. Fan, B. C. Daube, and S. C. Wofsy (1996), Measurements of carbon sequestration by long-term eddy covariance: methods and a critical evaluation of accuracy, *Glob. Change Biol.*, *2*(3), 169–182, doi:10.1111/j.1365-2486.1996.tb00070.x.

Grimmond, C. S. B., and T. R. Oke (1995), Comparison of Heat Fluxes from Summertime Observations in the Suburbs of Four North American Cities, *J. Appl. Meteorol.*, *34*(4), 873–889, doi:10.1175/1520-0450(1995)034<0873:COHFFS>2.0.CO;2.

Grimmond, C. S. B., T. S. King, F. D. Cropley, D. J. Nowak, and C. Souch (2002), Local-scale fluxes of carbon dioxide in urban environments: methodological

challenges and results from Chicago, *Environ. Pollut.*, *116*, S243–S254, doi:10.1016/S0269-7491(01)00256-1.

Hammerle, A., A. Haslwanter, M. Schmitt, M. Bahn, U. Tappeiner, A. Cernusca, and G. Wohlfahrt (2007), Eddy covariance measurements of carbon dioxide, latent and sensible energy fluxes above a meadow on a mountain slope, *Bound.-Layer Meteorol.*, *122*(2), 397–416, doi:10.1007/s10546-006-9109-x.

Holmes, H. A., J. K. Sriramasamudram, E. R. Pardyjak, and C. D. Whiteman (2015), Turbulent Fluxes and Pollutant Mixing during Wintertime Air Pollution Episodes in Complex Terrain, *Environ. Sci. Technol.*, *49*(22), 13206–13214, doi:10.1021/acs.est.5b02616.

Hong, J., J. Kim, D. Lee, and J.-H. Lim (2008), Estimation of the storage and advection effects on H2O and CO2 exchanges in a hilly KoFlux forest catchment, *Water Resour. Res.*, *44*(1), W01426, doi:10.1029/2007WR006408.

Horst, T. W. (1999), The Footprint for Estimation of Atmosphere-Surface Exchange Fluxes by Profile Techniques, *Bound.-Layer Meteorol.*, *90*(2), 171–188, doi:10.1023/A:1001774726067.

Hsieh, C.-I., G. Katul, and T. Chi (2000), An approximate analytical model for footprint estimation of scalar fluxes in thermally stratified atmospheric flows, *Adv. Water Resour.*, *23*(7), 765–772, doi:10.1016/S0309-1708(99)00042-1.

Judd, M. J., P. T. Prendergast, and K. J. McAneney (1993), Carbon dioxide and latent heat flux measurements in a windbreak-sheltered orchard, *Agric. For. Meteorol.*, *66*(3), 193–210, doi:10.1016/0168-1923(93)90071-O.

Kaimal, J. C., and J. C. Wyngaard (1990), The Kansas and Minnesota experiments, *Bound.-Layer Meteorol.*, *50*(1–4), 31–47, doi:10.1007/BF00120517.

Kantha, L. H., and C. A. Clayson (2000), *Small Scale Processes in Geophysical Fluid Flows*, Academic Press.

Kominami, Y., T. Miyama, K. Tamai, T. Nobuhiro, and Y. Goto (2003), Characteristics of CO2 flux over a forest on complex topography, *Tellus B*, *55*(2), 313–321, doi:10.1034/j.1600-0889.2003.00040.x.

Kramm, G., R. Dlugi, and D. H. Lenschow (1995), A re-evaluation of the Webb correction using density-weighted averages, *J. Hydrol.*, *166*(3–4), 283–292, doi:10.1016/0022-1694(94)05088-F.

Lareau, N. P., E. Crosman, C. D. Whiteman, J. D. Horel, S. W. Hoch, W. O. J. Brown, and T. W. Horst (2012), The Persistent Cold-Air Pool Study, *Bull. Am. Meteorol. Soc.*, *94*(1), 51–63, doi:10.1175/BAMS-D-11-00255.1.

Lee, X. H., and X. Z. Hu (2002), Forest-air fluxes of carbon, water and energy over non-flat terrain, *Bound.-Layer Meteorol.*, *103*(2), 277–301, doi:10.1023/A:1014508928693.

Mahrt, L., and R. Heald (2014), Common Marginal Cold Pools, *J. Appl. Meteorol. Climatol.*, *54*(2), 339–351, doi:10.1175/JAMC-D-14-0204.1.

Mahrt, L., D. Vickers, R. Nakamura, M. R. Soler, J. Sun, S. Burns, and D. H. Lenschow (2001), Shallow Drainage Flows, *Bound.-Layer Meteorol.*, *101*(2), 243–260, doi:10.1023/A:1019273314378.

Massman, W. J., and X. Lee (2002), Eddy covariance flux corrections and uncertainties in long-term studies of carbon and energy exchanges, *Agric. For. Meteorol.*, *113*(1–4), 121–144, doi:10.1016/S0168-1923(02)00105-3.

Moncrieff, J., R. Clement, J. Finnigan, and T. Meyers (2004), Averaging, Detrending, and Filtering of Eddy Covariance Time Series, in *Handbook of Micrometeorology*, edited by X. Lee, W. Massman, and B. Law, pp. 7–31, Springer Netherlands.

Mooney, H. A., P. M. Vitousek, and P. A. Matson (1987), Exchange of Materials Between Terrestrial Ecosystems and the Atmosphere, *Science*, *238*(4829), 926–932, doi:10.1126/science.238.4829.926.

Obukhov, A. M. (1971), Turbulence in an atmosphere with a non-uniform temperature, *Bound.-Layer Meteorol.*, *2*(1), 7–29, doi:10.1007/BF00718085.

Papadopoulos, K. H., and C. G. Helmis (1999), Evening and Morning Transition of Katabatic Flows, *Bound.-Layer Meteorol.*, *92*(2), 195–227, doi:10.1023/A:1002070526425.

Pattey, E., G. Edwards, I. B. Strachan, R. L. Desjardins, S. Kaharabata, and C. Wagner Riddle (2006), Towards standards for measuring greenhouse gas fluxes from agricultural fields using instrumented towers, *Can. J. Soil Sci.*, *86*(3), 373–400, doi:10.4141/S05-100.

Pielke, R. A., . Sr, R. Avissar, M. Raupach, A. J. Dolman, X. Zeng, and A. S. Denning (1998), Interactions between the atmosphere and terrestrial ecosystems: influence on weather and climate, *Glob. Change Biol.*, *4*(5), 461–475, doi:10.1046/j.1365-2486.1998.t01-1-00176.x.

Ramamurthy, P., and E. R. Pardyjak (2007), A comparison of CO2 fluxes at two sites within the urbanized Salt Lake Valley, *Seventh Symp. Urban Environ.*

Ramamurthy, P., and E. R. Pardyjak (2011), Toward understanding the behavior of carbon dioxide and surface energy fluxes in the urbanized semi-arid Salt Lake Valley, Utah, USA, *Atmos. Environ.*, *45*(1), 73–84, doi:10.1016/j.atmosenv.2010.09.049.

Raupach, M. R., A. S. Thom, and I. Edwards (1980), A wind-tunnel study of turbulent flow close to regularly arrayed rough surfaces, *Bound.-Layer Meteorol.*, *18*(4), 373–397, doi:10.1007/BF00119495.

Reid, K. H., and D. G. Steyn (1997), Diurnal variations of boundary-layer carbon dioxide in a coastal city—Observations and comparison with model results, *Atmos. Environ.*, *31*(18), 3101–3114, doi:10.1016/S1352-2310(97)00050-2.

Schmid, H. P. (2002), Footprint modeling for vegetation atmosphere exchange studies: a review and perspective, *Agric. For. Meteorol.*, *113*(1–4), 159–183, doi:10.1016/S0168-1923(02)00107-7.

Stannard, D. I., J. H. Blanford, W. P. Kustas, W. D. Nichols, S. A. Amer, T. J. Schmugge, and M. A. Weltz (1994), Interpretation of surface flux measurements in heterogeneous terrain during the Monsoon ’90 experiment, *Water Resour. Res.*, *30*(5), 1227–1239, doi:10.1029/93WR03037.

Stull, R. B. (1988), *An Introduction to Boundary Layer Meteorology*, Springer Science & Business Media.

Swinbank, W. C. (1968), A comparison between predictions of dimensional analysis for the constant-flux layer and observations in unstable conditions, *Q. J. R. Meteorol. Soc.*, *94*(402), 460–467, doi:10.1002/qj.49709440203.

Turnipseed, A. A., P. D. Blanken, D. E. Anderson, and R. K. Monson (2002), Energy budget above a high-elevation subalpine forest in complex topography, *Agric. For. Meteorol.*, *110*(3), 177–201, doi:10.1016/S0168-1923(01)00290-8.

U, K. T. P., D. D. Baldocchi, T. P. Meyers, and K. B. Wilson (2000), Correction Of Eddy-Covariance Measurements Incorporating Both Advective Effects And Density Fluxes, *Bound.-Layer Meteorol.*, *97*(3), 487–511, doi:10.1023/A:1002786702909.

Vickers, D., and L. Mahrt (2003), The Cospectral Gap and Turbulent Flux Calculations, *J. Atmospheric Ocean. Technol.*, *20*(5), 660–672, doi:10.1175/1520-0426(2003)20<660:TCGATF>2.0.CO;2.

Whiteman, C. D. (1982), Breakup of Temperature Inversions in Deep Mountain Valleys: Part I. Observations, *J. Appl. Meteorol.*, *21*(3), 270–289, doi:10.1175/1520-0450(1982)021<0270:BOTIID>2.0.CO;2.

Whiteman, C. D., and J. C. Doran (1993), The Relationship between Overlying Synoptic-Scale Flows and Winds within a Valley, *J. Appl. Meteorol.*, *32*(11), 1669–1682, doi:10.1175/1520-0450(1993)032<1669:TRBOSS>2.0.CO;2.

Wilczak, J. M., S. P. Oncley, and S. A. Stage (2001), Sonic Anemometer Tilt Correction Algorithms, *Bound.-Layer Meteorol.*, *99*(1), 127–150, doi:10.1023/A:1018966204465.

Wilson, K. et al. (2002), Energy balance closure at FLUXNET sites, *Agric. For. Meteorol.*, *113*(1–4), 223–243, doi:10.1016/S0168-1923(02)00109-0.

Yi, C., K. J. Davis, P. S. Bakwin, B. W. Berger, and L. C. Marr (2000), Influence of advection on measurements of the net ecosystem-atmosphere exchange of CO2 from a very tall tower, *J. Geophys. Res. Atmospheres*, *105*(D8), 9991–9999, doi:10.1029/2000JD900080.

Zhong, S., C. D. Whiteman, X. Bian, W. J. Shaw, and J. M. Hubbe (2001), Meteorological Processes Affecting the Evolution of a Wintertime Cold Air Pool in the Columbia Basin, *Mon. Weather Rev.*, *129*(10), 2600–2613, doi:10.1175/1520-0493(2001)129<2600:MPATEO>2.0.CO;2.